On the planetary forcing of the Solar dynamo: Evidence from a Lagrangian framework

Le Mouël Jean-Louis^{†1}, Courtillot Vincent¹, Vladimir Kossobokov^{2,3}, Gibert Dominique⁴, Lopes Fernando⁵, Boulé Jean-Baptiste⁵ and Zuddas Pierpaolo⁶

¹Académie des Sciences, Institut de France, Paris, France

²Institute of Earthquake Prediction Theory and Mathematical Geophysics, Russian Academy of Sciences, Moscow, Russia

³Accademia Nazionale delle Scienze detta dei XL, Roma, Italia

⁴DeepField Sensing, France

⁵Muséum National d'Histoire Naturelle, CNRS UMR7196, INSERM U1154, Paris, France

⁶Sorbonne Université, CNRS, METIS, UMR7619, Paris, France

[†]In Memoriam Jean-Louis Le Mouël passed away before the finalization of this manuscript. We dedicate this work to his memory.

Abstract

Whether planetary motions influence the solar magnetic cycle has remained an open question due to the lack of a rigorous physical mechanism. Here we develop a Lagrangian framework based on the Virial theorem to show that planetary orbital angular momentum modulates the Sun's rotation through barycentric dynamics, consistent with angular momentum conservation. Using Singular Spectrum Analysis (SSA) applied to sunspot number (SSN) and terrestrial length-of-day (LOD) records spanning the past 250 years, we identify two non-linear trends plus 11 common pseudo-cycles whose periods match those of planetary resonances (LR*). We then demonstrate that a reduced nonlinear $\alpha - \Omega$ dynamo model, forced solely by the summed planetary right ascension RA(t), reproduces both the Schwabe cycle and its multi-decadal envelope, including the Dalton Minimum and the Modern Maximum. These results provide strong evidence, based on a physically-grounded model, that the solar dynamo is weakly forced by planetary motion, suggesting that the solar dynamo, classically viewed as autonomous, may in fact behave as a synchronized system.

Keywords: Sunspot number (SSN), length-of-day (LOD), Virial theorem, planetary forcing, Solar dynamo.

1 Introduction

The idea that planetary motions might influence solar activity has been explored for over a century. Notably, Wolf (1859) suggested that the 11-year sunspot cycle (SSN, *cf.* Figure 1) could arise from the gravitational effects of Venus, Earth, Jupiter, and Saturn, sparking a debate that continues to this day. An approximately 11-year cycle whose multi-decadal envelope is strongly modulated over the past ~270 years (*eg.* Le Mouël *et al.* 2010), exhibiting marked minima in activity (blue region in Figure 1) as well as pronounced maxima (red region in Figure 1).

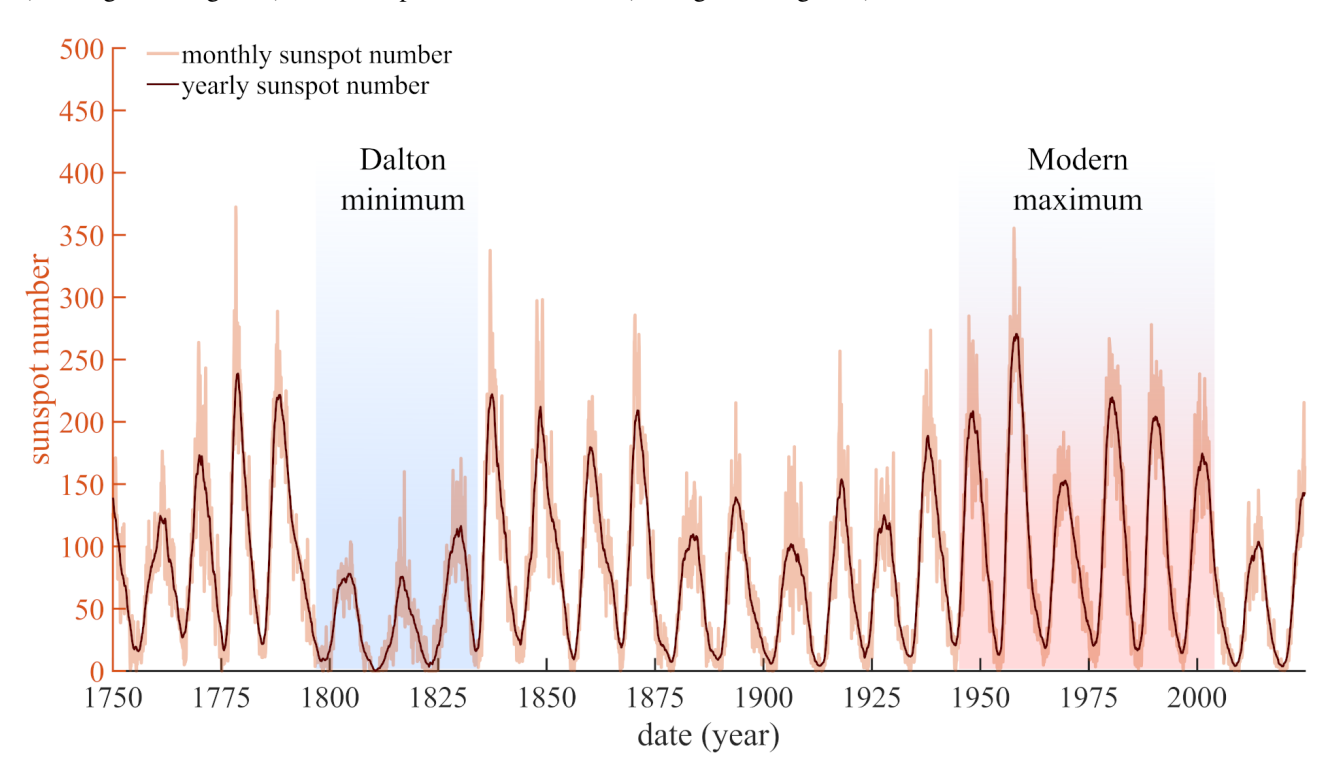


Figure 1: Evolution of the sunspot number series since 1749, shown as monthly values (in red) and annual averages (in black), as distributed by WDC-SILSO (2025). The record displays more than 24 complete Schwabe cycles (Schwabe 1844), with characteristic periods of approximately 11 years, varying between ~9 and ~13 years over time (*eg.* Courtillot et al. 2021). The amplitude envelope is also strongly modulated, revealing two prominent multi-decadal features: the Dalton Minimum (1800-1830; *ie.* low-activity shaded in blue) and the Modern Maximum (1945-2008; *ie.* high-activity shaded in red).

The concept of planetary influence is well-established in geophysics, particularly as regards variations in the length-of-day (LOD). The Sun, the Moon, and Jupiter are the most significant candidates as contributors to these variations (*eg.* Lambeck 2005, Le Mouël *et al.* 2019, Lopes *et al.* 2021). It has also long been recognized that there is a link between sunspot activity, as estimated by variations in the Sunspot Number (SSN), and fluctuations in the LOD. This relationship is attributed in general to solar insolation with thermal contrasts between distinct regions driving winds. These winds can perturb Earth's rotation (*eg.* Rosen & Salstein 1983, del Rio *et al.* 2003, Lopes *et al.* 2017, Le Mouël *et al.* 2019), through exchanges of angular momentum at the atmosphere/solid Earth interface. However, these exchanges are almost negligible. As noted in previous studies, solar irradiance has remained essentially constant over the past few centuries. Pouillet (1837) was the first to measure what is now known as the "solar constant", estimating it at 1230 W· m⁻². Today, this value is estimated to be approximately 1366 W· m⁻², exhibiting only minor fluctuations, on the order of 0.1% to 0.3%, over the

course of the 11-year solar cycle (eg. Eddy et al. 1982, Kuhn et al. 1988, Li et al. 2012). Laplace (1799) had already anticipated this observation in his treatise on Celestial Mechanics (eg. Chao et al. 2014, Ray & Erofeeva 2014, Sidorenkov 2017). Here, we attempt to address these criticisms by formulating a concrete physical coupling mechanism and by testing its consistency with observations.

The main solar periodicities reported in the literature that could be connected to planetary orbital features are:~160 years (the Jose (1965)' cycle/Neptune), ~90 years (the Gleissberg (1939)' cycle/Uranus), ~60 years, ~33 years (Saturn),~28 years (Jupiter + Saturn + Uranus, cf. Le Mouël et al. (2023)), ~22 years (the Hale et al. (1919)' cycle), then ~19 years, ~9 and 14 years (the Schwabe (1844)' cycle/Jupiter), ~5.5 years, and ~3.6 years (harmonics of Schwabe cycle). Many of these cycles have loosely been identified across a wide range of geophysical phenomena (eg. Bartels 1932, Zaccagnino et al. 2020, Courtillot et al. 2022, Le Mouël et al. 2023, Diodato & Bellocchi 2024, Dumont et al. 2025, Xiao et al. 2025). The mechanisms that could explain them remain hypothetical. They include internal geophysical processes, the solar dynamo, planetary tidal forces, and oscillations of the Sun around the barycenter of the solar system (cf. Wood & Wood 1965, Smythe & Eddy 1977, Fairbridge & Shirley 1987, Charvátová 1988, Seymour et al. 1992, Hung 2007, Perryman & Schulze-Hartung 2011, Stefani et al. 2016, Cionco & Pavlov 2018, Stefani et al. 2019, Courtillot et al. 2021, Scafetta & Bianchini 2022, Shirley 2023). This last point is of particular importance, as the total planetary orbital angular momentum, or its barycentric projection, is significant; it actively alters the Sun's angular momentum about the barycenter (eg. Jose 1965).

The debate on the likelihood of such mechanisms remains lively. The planetary forcing hypothesis has met with skepticism, because no convincing physical coupling has been identified and the tidal forces that planets exert on the Sun appear far too small compared to the forces driving its internal dynamo. Jupiter, the most massive planet, would generate a tidal acceleration of only $10^{-10}m.s^{-2}$, producing a surface deformation of roughly 0.1 mm, that is negligible compared to solar gravity and rotational stresses (*cf.* Callebaut *et al.* 2012). As another example, no significant correlation has been found between the helio-longitude of sunspot emergence and planetary positions, apparently reinforcing the view that the solar magnetic cycle is primarily an internal phenomenon (*eg.* Seker 2013).

In this study, we revisit this longstanding question by introducing a novel physical framework rooted in classical mechanics, combined with a new quantitative analysis of key heliophysical and geophysical observations. In the first part, Section 2.1, we rely on the formalism of classical mechanics developed by (Lagrange, 1788), complemented by the Virial Theorem (*cf.* Appendix A), to describe the dynamics of the Sun within the planetary system, and, by extension, the dynamics of sunspot activity. From this perspective on Lagrangian mechanics through the Virial theorem, we derive the full expression for the total mean orbital angular momentum of the planets in our solar system, whose simple Fourier analysis already reveals the expected set of characteristic periods. In Section 3, we then jointly analyze the time series of the LOD variations (*eg.* Courtillot 1978, Holme & De Viron 2013, Duan *et al.* 2015) since 1780 and the SSN since 1750 using Singular Spectrum Analysis (SSA), with the goal of extracting their shared pseudo-cyclic components. By pseudo-periodicity, we refer to a mono-modal oscillatory signal whose phase and amplitude evolve over time. This analysis shows that these two physical phenomena share 12 common components (*eg.* Jose 1965, Mörth & Schlamminger

1979, Courtillot *et al.* 2021), a trend and 11 highly correlated periods (*cf.* Table 2). We conclude this section (*cf.* 3.3) with a detailed presentation of a simplified nonlinear dynamo model, externally forced by the right ascensions, whose output accounts for a significant portion of the temporal evolution of the sunspot number (*eg.* Usoskin 2017, Scafetta 2012, Scafetta 2014, Stefani *et al.* 2021, Horstmann *et al.* 2023, Stefani *et al.* 2024). Finally, Section 4 presents an in-depth discussion of our results and reconsiders the broader question of a possible planetary forcing of solar activity.

2 Theoretical framework

2.1 The Virial theorem

We follow a Lagrangian mechanics approach (*eg.* Landau & Lifshitz 2000, Lopes *et al.* 2022) to the Sun-planet system. By applying the Virial theorem (*cf.* Lagrange 1788, Appendix A) to the solar interior under external planetary perturbations, one can derive how orbital forces could affect solar kinetic and potential energy balance.

The Virial theorem states broadly that in a gravitationally bound system the average kinetic energy is proportional to the average potential energy. Over long timescales, the system oscillates about an equilibrium state without any net gain or loss of energy. From this perspective on Lagrangian mechanics and the Virial theorem, one can derive the full expression for the total mean orbital angular momenta ($\langle M_{tot} \rangle$) of the planets.

Consider a system of N planets with masses m_i , including the Sun, subject only to gravitational interaction. The system is closed, ie, there is no exchange of energy or angular momentum with the outside. In the long term, the system satisfies the Virial theorem: there is a continuous exchange between the total kinetic and potential energies of the system, without dissipation.

Let T be the total kinetic energy and U the total gravitational potential energy of a system. The governing equations of such a system are given by,

$$2\langle T \rangle = \langle U \rangle \Longrightarrow \langle E \rangle = \langle T \rangle + \langle U \rangle = -\langle T \rangle < 0, \tag{1a}$$

$$M_{tot} = \sum_{i=1}^{N} (m_i \mathbf{r}_i \times \mathbf{v}_i) + I_i \mathbf{\Omega}_i$$
 (1b)

where $\langle . \rangle$ represents averaging over a long time span, $\langle E \rangle$ denotes the total energy of the system, expressed through its Lagrangian formulation. (1a) refers to the Virial theorem applied to a gravitational potential of the form 1/r, which implies that the long-term mean total energy is negative, thus confirming that the system remains gravitationally bound. The Virial analysis provides a physical basis for planetary-solar coupling, a mechanism thanks to which planets might influence solar activity, thus addressing a key criticism from past studies. This classical mechanics approach will allow us to quantify how even tiny exchanges of angular momentum, otherwise dismissed as negligible, could have tangible effects on solar rotation

and magnetism.

2.2 A Galilean barycentric reference frame

A Galilean barycentric reference frame is a coordinate system commonly used to describe the motion of a collection of celestial bodies. The barycenter of a system of bodies is its common center of mass. In the case of the solar system, where the Sun dominates in mass, the barycenter is not located precisely at the Sun's geometric center, but is slightly displaced due to the gravitational influence of the planets, particularly the giant planets Jupiter and Saturn. As a result, the barycenter sometimes lies within the Sun and at other times outside of it, depending on the orbital configuration of the planets (*cf.* Figure 2). The second essential aspect of this reference frame is its Galilean nature, meaning that it is not subject to any external acceleration or force. This barycenter of the system (Sun + planets) is defined by,

$$\mathbf{R}_b = \frac{\sum_{i=1}^N m_i \mathbf{r}_i}{\sum_{i=1}^N m_i} \tag{2}$$

2.3 Considerations on angular momentum transfer

Let M_{tot} stand for the total angular momentum of the planetary system relative to the Sun, consisting of an orbital component (M_{orb}) and a rotational component (M_{rot}) . The orbital angular momentum (M_{orb}) of each planet is defined by two vectors, position and velocity relative to the Sun. The rotational angular momentum (M_{rot}) , on the other hand, is given by the product of the planet's moment of inertia I and its angular velocity Ω . In a Galilean barycentric reference frame, the first time derivative of equation (1b) must be zero. Appendix B discusses the consequences of angular momentum transfer between the planets.

Although the Sun contains $\sim 99.9\%$ of the solar-system mass, the orbital angular momentum budget is dominated by the four Jovian planets that together carry roughly 95 - 99% of the total, with Jupiter alone exceeding 60% (cf. Table 1).

Body	Mass (kg)	Radius (m)	Revolution (days)	Rotation (s)	Inertia Factor	Aphelia (m)
Sun	1.989×10^{30}	6.957×10^{8}	_	2.16×10^{6}	0.070	_
Mercury	3.301×10^{23}	2.4397×10^6	87.97	5.07×10^{6}	0.346	5.79×10^{10}
Venus	4.867×10^{24}	6.0518×10^6	224.7	2.10×10^{7}	0.337	1.082×10^{11}
Earth	5.972×10^{24}	6.371×10^6	365.25	8.62×10^4	0.331	1.496×10^{11}
Mars	6.417×10^{23}	3.3895×10^6	687.0	8.88×10^{4}	0.366	2.279×10^{11}
Jupiter	1.898×10^{27}	6.9911×10^7	4331	3.57×10^4	0.254	7.785×10^{11}
Saturn	5.683×10^{26}	5.8232×10^7	10747	3.78×10^4	0.220	1.433×10^{12}
Uranus	8.681×10^{25}	2.5362×10^7	30589	6.20×10^4	0.230	2.877×10^{12}
Neptune	1.024×10^{26}	2.4622×10^7	59800	5.80×10^{4}	0.250	4.503×10^{12}

Table 1: Fundamental physical constants for the Sun and planets used in this study

The conservation of the total momentum of the system, provided there are no external forces, implies that the barycenter

moves in a straight line at constant velocity. This barycentric reference frame is often considered to be at rest for simplicity. In that case, it is the Sun itself (M_{\odot}) that traces a small orbit around this barycenter as its planets change position. If a planet m_i slightly changes its angular momentum, eg. through planetary interactions such as resonances or torques, the total angular momentum M_{orb} (eg. relation 1b) must remain constant. Part of the variation is therefore transferred to the orbital angular momenta of the other planets, the Sun's orbital motion around the barycenter, or the spin axis (eg) intrinsic rotation) of the planet or the Sun (since internal rotation also contributes to the total angular momentum).

2.4 Trajectory of the Solar system barycenter

In a barycentric reference frame, the position of the Sun is \mathbf{r}_{\odot} . Because the system is closed and the barycenter moves at constant velocity, the Sun of mass M_{\odot} describes a small orbit around it, governed by the gravitational attractions from all planets. From Newton's second law, the acceleration of the Sun satisfies,

$$M_{\odot}\ddot{\mathbf{r}}_{\odot} = -\sum_{j} \mathcal{G}M_{\odot}m_{i} \frac{\mathbf{r}_{\odot} - \mathbf{r}_{j}}{\|\mathbf{r}_{\odot} - \mathbf{r}_{j}\|^{3}}$$
(3)

where the index j runs over the N planets. This relation is the direct analogue of the orbital motion equation for a planet, now applied to the Sun. As discussed, it ensures that the total angular momentum remains constant (cf. equation 1b) and that the Virial condition (cf. equation 1a) is not violated by internal transfers of momentum.

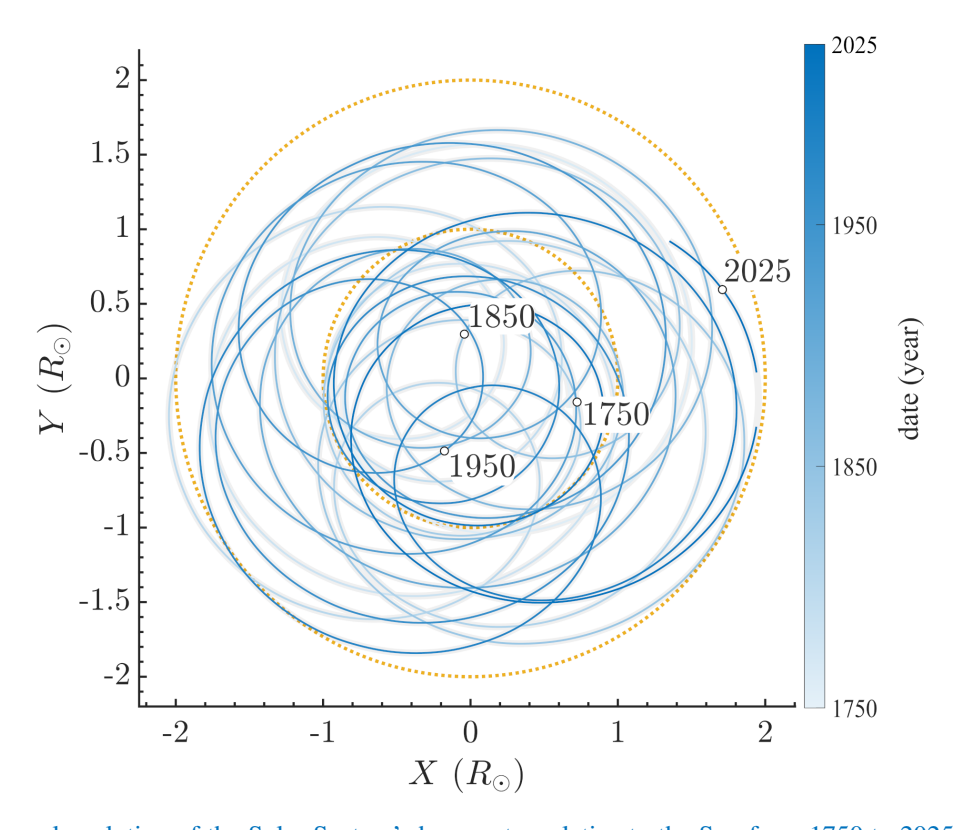


Figure 2: Temporal evolution of the Solar System's barycenter relative to the Sun from 1750 to 2025, computed in a Galilean barycentric reference frame using planetary ephemerides provided by the IMCCE (*ie.* Institut de mécanique Céleste et de Calcul des Ephémérides). The trajectory, displayed in the XY plane and expressed in solar radii (R_{\odot}), transitions in color from light blue (1750) to dark blue (2025). It shows that, under the gravitational influence of the planets, the barycenter has migrated by nearly two solar radii over the past three centuries, as indicated by the dashed yellow circles.

Figure 2 shows the evolution of the Solar System's barycenter relative to the Sun over a 200-year period. The trajectories were computed using equation (3), based on planetary ephemerides provided by the *Institut de Mécanique Céleste et de Calcul des Ephémérides* (IMCCE¹). The Newtonian influence of the planets is sufficient for the barycenter to move up to twice the solar radius. The kinetic energy associated with the Sun's motion around the barycenter is linked to the gravitational potential energy due to the planets through the Virial relation (equation 1a). The Sun oscillates around an equilibrium position dictated by the distribution of planetary masses. In other words, the Sun's barycentric oscillations can be interpreted as normal modes of the planetary system, and the Virial theorem ensures that these oscillations remain bounded (*ie.* the Sun does not escape).

Let $L_{\odot}(t)$ denote the Sun's orbital angular momentum about the barycenter, which is equal and opposite to the total orbital angular momentum of the planets. To better assess the impact of M_{tot} on the Sun, and consequently on its sunspots, we will compute the Sun's orbital angular momentum about the barycenter,

$$\underbrace{M_{\odot}\mathbf{r}_{\odot} \times \mathbf{v}_{\odot}}_{\mathbf{L}_{\odot}} + \underbrace{\sum_{i} m_{i}\mathbf{r}_{i} \times \mathbf{v}_{i}}_{M_{tot} - \Sigma_{i}, \mathbf{l}_{i}\Omega_{i}} + C \text{ constant}$$

$$(4)$$

We remove the constant vector C from \mathbf{L}_{\odot} and $\sum_{i} \mathbf{L}_{i}$ to analyse fluctuations about the barycentric constant of motion. This operation follows angular-momentum conservation. Thus, we can write,

$$\mathbf{L}_{\odot}(t) \approx -\sum_{i} \mathbf{L}_{i}(t) \tag{5}$$

Therefore, the variations in $\mathbf{L}_{\odot}(t)$ are opposite to those of the planetary sum $\sum_{i} \mathbf{L}_{i}(t)$. Note that the $\sum_{i} \mathbf{I}_{i}\Omega_{i}$, which are not included here, is nonetheless several orders of magnitude smaller than the total planetary angular momentum $\sum_{i} \mathbf{L}_{i}(t)$.

Any change in the orbital momentum of the planets must be compensated by a change in the Sun's rotational momentum, spin or orbital motion about the barycenter. In practice, as we discuss later, the relative orientation of the planets, which can be tracked via their combined Right Ascension signal, will modulate the Sun's rotation rate.

3 Methods and Results

3.1 $L_{\odot}(t)$, LOD and SSN: data and methods

Following the approach of Section 2, we computed the total orbital angular momentum $\mathbf{L}_{\odot}(t)$ of the planetary system (Sun about the barycenter). Because the total angular momentum is conserved (*cf.* relation 4), $\mathbf{L}_{\odot}(t)$ varies only slightly

¹https://vo.imcce.fr/webservices/miriade/?forms

around a constant mean. We focus on these small fluctuations (*cf.* Figures 3b and 4b). One way to highlight the spectral richness of $\mathbf{L}_{\odot}(t)$ is also to define a combined planetary alignment index, noted $RA_{\text{tot}}(t)$, as the mass-weighted sum of the planets' instantaneous right ascensions in an inertial frame. More explicitly,

$$RA_{\text{tot}}(t) = \sum_{i=1}^{N} m_i RA_i(t),$$

where $RA_i(t)$ is the heliocentric right ascension (in degrees) of planet i at time t, and m_i its mass. This aggregated angular index, shown in Figures 3a and 4b, offers a compact measure of the evolving planetary configuration.

As shown, $\mathbf{L}_{\odot}(t)$, represented by the red curve in Figure 3b, exhibits a much smoother and more monotonic behavior than (blue curve, Figure 3a), which displays a characteristic saw-tooth pattern. The corresponding Fourier spectra are presented in Figure 3b for $\mathbf{L}_{\odot}(t)$ and in Figure 2d for RA_{tot} . We have indicated in dark red, approximately, the main periods that can be visually identified in the spectra. Given the different nature of the time series, the amplitudes of the Fourier spectra differ; nevertheless, the main periodicities are preserved. All these periodicities correspondo those known in the sunspot record, for instance, ~11 yr (Schwabe cycle) and ~22 yr (Hale double cycle) *etc.*, as documented Le Mouël *et al.* (2020a).

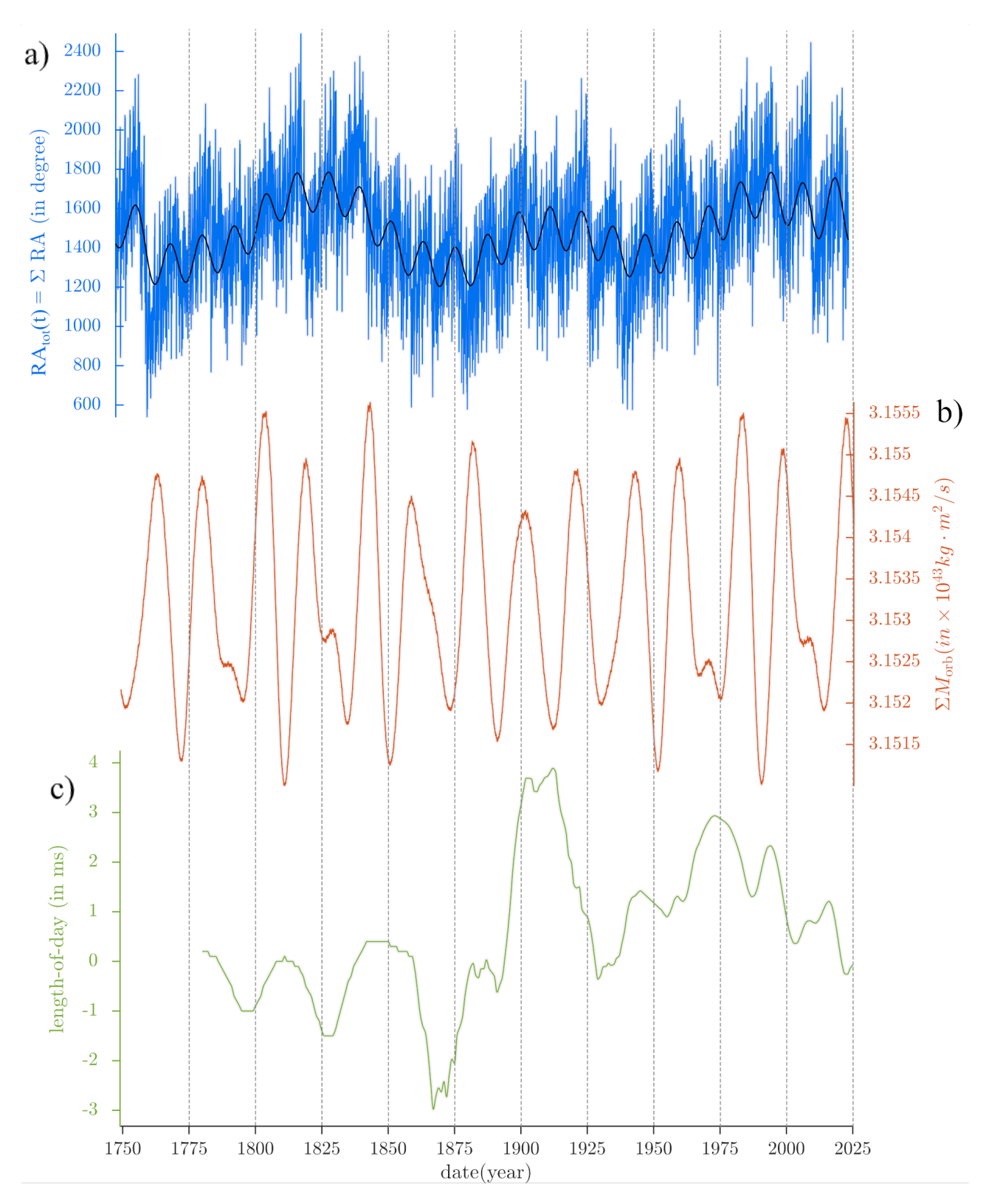


Figure 3: Temporal evolution of astronomical and geophysical data. The upper panel (blue) shows the sum of planetary right ascensions (RA_{tot}), and the middle panel (red) displays the total orbital angular momentum ($\mathbf{L}_{\odot}(t)$), both computed from planetary ephemerides since 1750. The lower panel (green) presents the geophysical variable, the length-of-day, from 1780 onward, based on the reconstructed series of Stephenson and Morrison (1984) and extended by satellite-based measurements provided by the IERS from 1962 to the present.

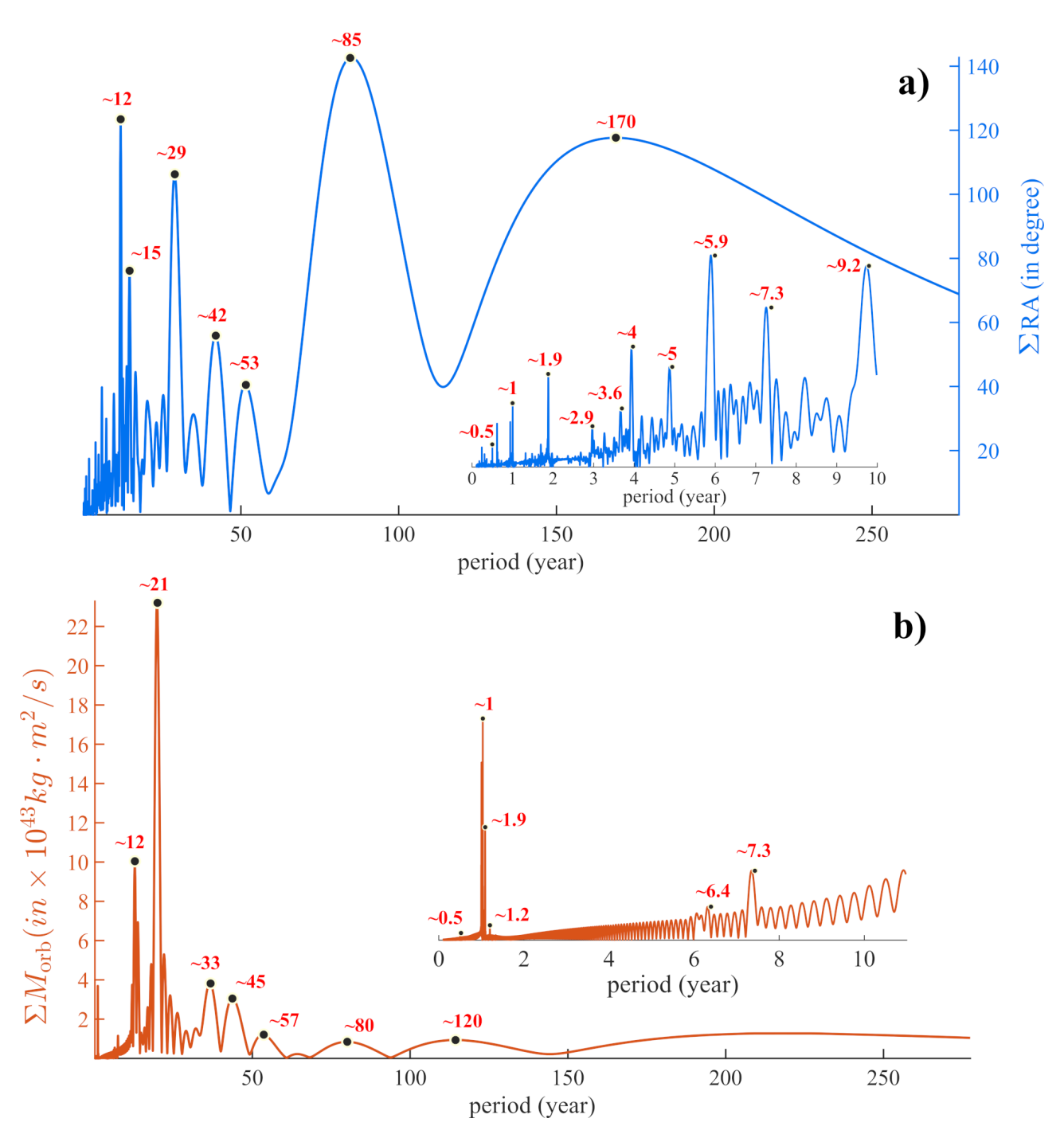


Figure 4: Fourier spectra, expressed in periods, of (a, blue) the summed planetary right ascensions and (b, red) the summed orbital angular momenta. Clear common periodicities emerge in both series, although their relative amplitudes differ, as expected given their distinct physical nature. These periodicities correspond not only to the planets' orbital periods but also to their Laplace-type resonances (LR^*). They are also identical to those observed in the sunspot number record (cf. Table 2).

3.2 Total momenta, LOD and SSN: power spectra and SSA components

We next compare the power spectra of the monthly sunspot numbers record (from WDC-SILSO, Royal Observatory of Belgium) and LOD variations with that of the total moment (*cf.* Table 2). LOD is a reconstructed series of Stephenson and Morrison (1984) and extended by satellite-based measurements provided by the IERS from 1962 to the present. LOD (*cf.* Figure 3b, in green) is used here as an independent proxy for external influences (*eg.* planetary tidal forces or angular

momentum exchanges) acting on Earth's rotation (*eg.* del Rio *et al.* 2003). In the present study, the Singular Spectrum Analysis method detected a trend and 11 pseudo-periodic components in all three datasets and these twelve components are identical from one data set to the other. These pseudo-periods account for 48.8% of the reconstructed energy in the LOD series and 50.2% of the reconstructed energy in SSN. The method we used to separate all pseudo-oscillatory components, SSA, also has its limitations (*cf.* Lopes *et al.* 2024). Given the spectrum of $\mathbf{L}_{\odot}(t)$ (*cf.* Figure 4b), certain periods are difficult to discern, even though we know they are present; since $\mathbf{L}_{\odot}(t)$ includes $RA_{tot}(t)$, and we do detect them in the latter. The reason is straightforward: the planetary weightings, often linked to planetary mass, tend to favour the Jovian planets and their associated torques over those of the terrestrial planets.

In the case of the sunspot series SSN, the shortest cycle we could robustly extract is \sim 3.6 years. This suggests that approximately 50% of the SSN variance lies in fluctuations with periods below \sim 3-4 years (which are beyond the scope of our SSA analysis focused on decadal-and-longer scales).

SSN (yr)	LOD (yr)	L_{\odot} (yr)	LR*
trend	trend		might represent a portion of a (~550)-yr cycle
(~ 182.42)	(~ 186.2)	200 ± 45	de Vries cycle / Neptune (164.89 yr)
(77.71 ± 13.63)	(83.25 ± 17.83)	81.36 ± 5.47	Gleissberg cycle / Uranus (84.01 yr)
(54.38 ± 16.2)	(50.36 ± 9.09)	56.83 ± 2.11	Neptune + Uranus (57.29 yr)
(34.35 ± 2.79)	(32.63 ± 2.84)	33.15 ± 1.58	Jupiter + Uranus (36.06 yr)
(26.81 ± 2.04)	(27.6 ± 3.33)	28.95 ± 1.26	Jupiter + Saturn + Uranus (25.57 yr)
(21.25 ± 1.03)	(22.27 ± 1.30)	21.06 ± 1.02	Hale cycle / Jupiter + Saturn (21.64 yr)
(18.23 ± 1.09)	(19.37 ± 1.11)	20.03 ± 0.33	Jupiter + Saturn (18.61 yr)
(13.12 ± 0.38)	(13.26 ± 0.44)	14.15 ± 0.23	Schwabe cycle / Jupiter (11.85 yr)
(11.01 ± 0.33)	(10.45 ± 0.37)	11.92 ± 0.25	Schwabe cycle / Jupiter-Saturn (9.31 yr)
(5.48 ± 0.07)	(5.34 ± 0.17)	5.81 ± 0.12	Jupiter (5.92 yr)
(3.88 ± 0.03)	(3.61 ± 0.03)	3.60 ± 0.10	Jupiter (3.91 yr)

Table 2: Common pseudo-periods associated with the detected and extracted pseudo-cycles. In the planetary resonance (LR^*) column, the names of the solar cycles corresponding to the detected periods are given, along with the main planets associated with these cycles according to Mörth and Schlamminger (1979). In red are indicated the periods that are not detected by our method in L_{\odot} but are clearly detected in RA_{tot} .

For each pseudo-cycle, the nominal periodicity (P_n) was computed using a simple Fourier transform. The associated error bar corresponds to the full width at half maximum of the sinc-function centered on P_n . Rather than presenting the LOD components as directly extracted, except for the trend (cf. Figure 5a) we show their time-integrated form, since the LOD is often interpreted as a derivative of the external torques acting upon it (eg. Lambeck 2005, Lopes et al. 2022). Figures 5 and 6 present, in decreasing order of period, the trend and 11pseudo-cycles components to both time series, extracted by optimized Singular Spectrum Analysis (SSA, cf. Lopes et al. 2024). Throughout, components associated with LOD are shown in blue, while those related to sunspot activity are shown in red.

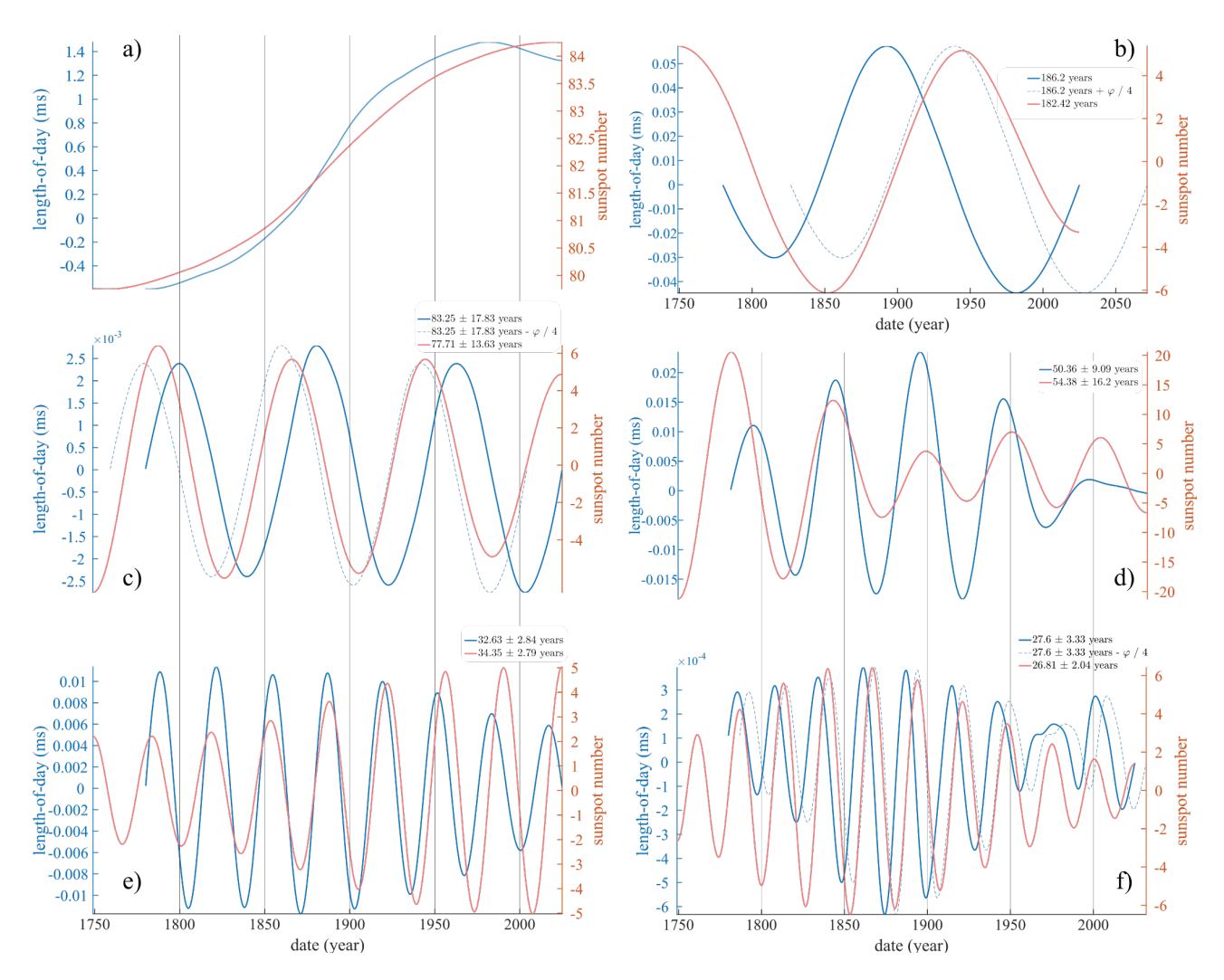


Figure 5: Superposition of the pseudo-cycles extracted from the sunspot number series (in red) and their counterparts from LOD variations (in blue) for: (a) the trend, (b) the \sim 182-year pseudo-cycle associated with the de Vries cycle, (c) the \sim 80-year pseudo-cycle associated with the Gleissberg cycle, (d) the \sim 60-year pseudo-cycle, (e) the \sim 33-year pseudo-cycle, and (f) the \sim 27-year pseudo-cycle.

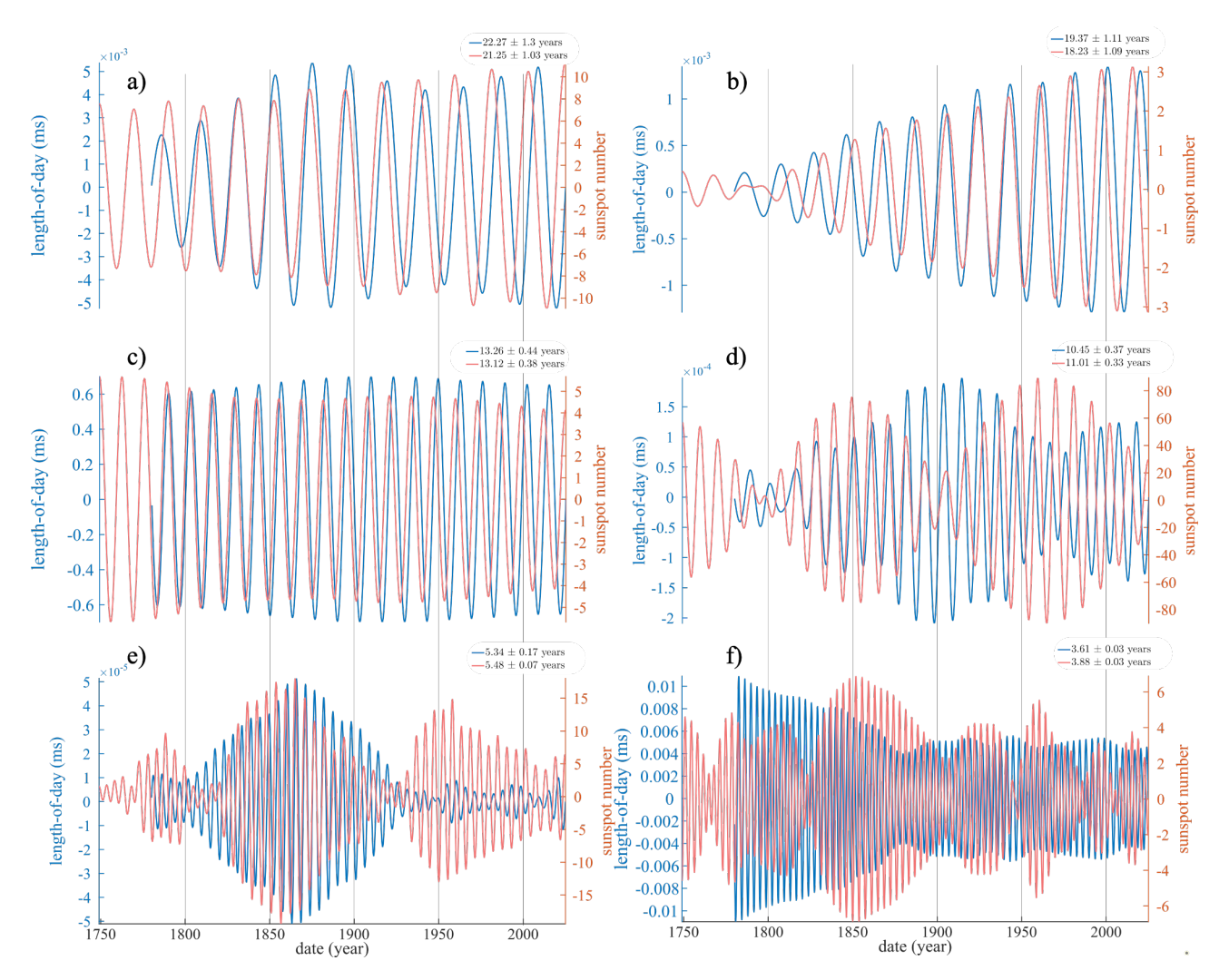


Figure 6: Superposition of the pseudo-cycles extracted from the sunspot number series (in red) and their counterparts from LOD variations (in blue) for: (a) the \sim 22-year pseudo-cycle associated with the de Hale cycle, (b) the \sim 19-year pseudo-cycle, (c) the \sim 13-year pseudo-cycle associated with the Schwabe cycle, (d) the \sim 11-year pseudo-cycle associated with the Schwabe cycle, (e) the \sim 5.5-year pseudo-cycle, and (f) the \sim 3.6-year pseudo-cycle.

Figures 5 and 6 highlight several noteworthy aspects regarding the behavior of the phases and envelopes of the pseudo-cycles over time. Starting with the trend component (*cf.* Figure 4a), both physical variables exhibit increasing sigmoid-like patterns. These could represent segments of monotonous trends on millennial time scales but they could alternately correspond to components with a much longer period, approximately 550 to 600 years. This might correspond to a pseudo-cycle previously identified in the record of terrestrial volcanic eruptions (*cf.* Le Mouël *et al.* 2023), as well as in the growth rates of juniper tree rings from the Tibetan Plateau (*cf.* Courtillot *et al.* 2023). The SSN trend has reached a plateau since the early 2000s, while the LOD trend has been decreasing since the mid-1980s. This divergence has gradually led to what is now recognized, since 2020, as an acceleration in the Earth's rotation (*cf.* Trofimov *et al.* 2021).

Next comes the de Vries cycle (~182 years; *cf.* . Figure 4b; *eg.* Wagner *et al.* 2001, Stefani *et al.* 2019), whose uncertainty range, given the low number of observable cycles, is difficult to determine in the Fourier domain. However, it is known to be at least greater than 40 years. As shown in the figure, if one applies a phase quadrature shift ($\varphi/4 \approx 46$ years), the two waveforms, dashed blue and red, become nearly superimposed. The next extracted pseudo-cycle corresponds to the

Gleissberg (1939) cycle (cf. Figure 5c), with a period of approximately 84 years (cf. Le Mouël et al. 2017). In this case, the number of cycles is sufficient to estimate an uncertainty range: ±17.8 years for LOD and ±13.6 years for SSN. Once again, a phase quadrature shift (~21 years) was applied, resulting in the two waveforms aligning closely and exhibiting coherent behavior. The next pseudo-cycle (cf. Figure 5d) is the ~60-year cycle, which has been frequently identified in climatic and geomagnetic variations (eg. Veretenenko & Ogurtsov 2018, Ptitsyna & Demina 2021), as well as in meteorite occurrence records (eg. Scafetta et al. 2020). In this case, the associated uncertainty ranges are ±9 years for LOD and ±16 years for SSN. Unlike the three previous cycles, the phases and amplitudes here do not align as closely. A slight phase drift appears to emerge over time, even though the oscillatory patterns remain relatively similar. However, regarding their envelopes, the waveform associated with sunspot activity shows a clear decreasing trend over time. A slight phase shift over time is also observed in the next pseudo-cycle (~33 years; cf. . Figure 5e). First identified by Schove (1947) in SSN, this cycle has also been reported on Earth, for example, in variations of the geomagnetic field (cf. Courtillot et al. 1977) and in dendrochronological records from northern Russia (cf. Kasatkina et al. 2007). At present, this cycle is thought to possibly result from nonlinear superpositions of fundamental solar cycles (11 and 22 years), from internal dynamic processes within the Sun, or from external planetary forcing, similar to hypotheses proposed for the ~60-year cycle associated with Jupiter and Saturn.

Next is the \sim 27-year cycle (*cf.* Figure 5f), which, like the first three pseudo-cycles, exhibits striking characteristics: the evolution of both envelopes and phases is nearly superimposable over time when a phase quadrature shift is applied (dashed blue curve). This cycle was first documented by Willett (1962), who correlated ozone variability with this solar cycle.

The following cycles exhibit several tens of repetitions over the 1750-2025 period. However, it is well known that even if two signals are theoretically synchronous, in practice, due to phase drift or, as in this case, due to SSA-based extraction, phase delays may be introduced, as the recovered periods are no longer exactly identical (*eg.* Gardner 1993, Latt *et al.* 2009). Therefore, for the subsequent cycles, we remain cautious regarding any putative phase quadrature relationships or observed phase drifts.

Figure 6a shows the ~22-year pseudo-cycles extracted from the LOD and SSN series. The associated uncertainty ranges are relatively small: ±1.3 years for LOD and ±1 year for SSN. This cycle, first described by Hale *et al.* (1919), is thought to be directly related to the Sun's global magnetic field, which reverses polarity every 11 years, resulting in a complete 22-year magnetic cycle. The phases of the two components are generally close, although a slight shift emerges over time. In Figure 6b, the following pair of pseudo-cycles, centered around 19 years, show remarkably similar amplitudes, with their envelopes increasing in mirrored fashion since 1800. A phase drift is also observed: LOD leads SSN until around 1900, followed by perfect phase alignment up to 1950, after which LOD lags behind SSN. The presence of this cycle in the SSN series with such clarity is somewhat surprising, as it is traditionally associated with LOD and attributed to the 18.6-year lunar nodal cycle, the precession of the Moon's orbital plane, which affects terrestrial ocean tides. Interestingly, recent studies have also linked this periodicity to the Jupiter–Saturn conjunction cycle, suggesting a possible modulation of solar activity through gravitational tidal effects (*eg.* Scafetta & Bianchini 2022). The next two cycles, ~14 years (*cf.* Figure 6c) and ~11 years (*cf.* Figure 6d), clearly correspond to the Sun's principal cycle, known as the Schwabe (1844) cycle, which

is known to vary between 9 and 14 years (*eg.* Richards *et al.* 2009, Courtillot *et al.* 2021). For the first pseudo-cycles, we find periods of 13.26±0.44 years for LOD and 13.12±0.38 years for SSN. For the second pseudo-cycles, the values are 10.45±0.37 years for LOD and 11.01±0.33 years for SSN. Within the margin of error, the periods of both cycles are essentially the same in the two datasets. Additionally, the evolution of their envelopes is nearly identical for the ~14-year pseudo-cycle, while for the ~11-year pseudo-cycle, both series exhibit similar amplitude modulations (beating patterns), although slightly shifted in time. Figure 6e shows the ~5.5-year pseudo-cycles. This cycle is frequently observed in time series related to solar activity (*eg.* Mursula *et al.* 1997), the geomagnetic field (*eg.* Currie 1966), and certain climatic variables (*eg.* Le Mouël *et al.* 2019). It is often interpreted either as a harmonic of the Schwabe (1844) cycle or as an independent signal of still-debated origin. The waveforms exhibit beat patterns with a period of approximately 130 years, with two such beats, one in the LOD and the other in the SSN series, remarkably coinciding between 1800 and 1925. We conclude this list of pseudo-cycles with the ~3.6-year cycle (*cf.* Figure 6f). This periodicity has been identified in geomagnetic indices (*eg.* the *Ap* index, *cf.* Tsichla *et al.* 2019) as well as in surface temperature variations (*cf.* Mufti & Shah 2011, Le Mouël *et al.* 2020b). The only clear observation in this case is that the amplitude of the waveforms decreases over time.

We have just shown that SSA analysis of LOD and SSN, two time series that, *a priori*, are not expected to be related, reveals the presence of 11 common pseudo-cyclicities shared between these two physical systems. Furthermore, thanks to SSA's ability to reconstruct the temporal evolution of individual waveform components, it becomes apparent that several of these cyclicities are nearly identical, differing only by a phase quadrature. Such coherence is unlikely to be coincidental. These 11 pseudo-cycles account for approximately half of the total variance in each time series and correspond strictly to the periods found in the sum of the mean orbital angular momenta (*cf.* Figure 2 and Table 2 At this stage, it appears reasonable to hypothesize that the orbital angular momenta (*cf.* Equation 1b) may exert a forcing, at least in part, on both SSN and LOD variability.

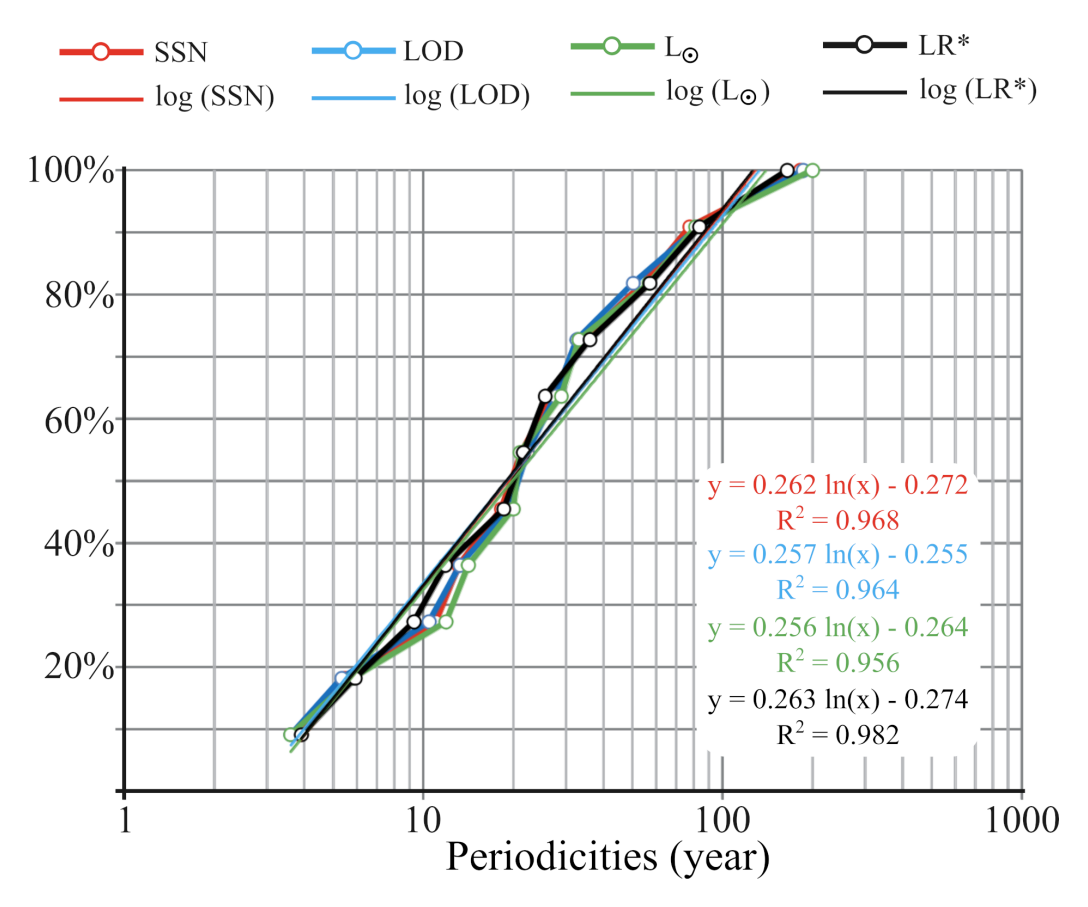


Figure 7: The empirical cumulative distribution functions of detected periodicities from SSN (red curve), LOD (blue curve), L_{\odot} (green curve), and the reference distribution for Laplace-type resonances (LR^*) (black curve).

We found that the correlation between the 11 extracted periods in SSN and LOD reaches 99.9%. Using bootstrap simulations (cf. Appendix C), we estimate that the probability of obtaining such a high correlation by chance is $\leq 10^{-3}$. This confirms that the common periods identified are very unlikely to result from coincidence. Furthermore, the close alignment of the empirical cumulative distributions of SSN, LOD, and the solar orbital angular momentum L_{\odot} with the theoretical reference distribution LR^* (cf. Figure 7, Appendix C) provides independent statistical confirmation that these periodicities may not arise from different processes. Taken together, these incredibly good results provide compelling evidence for the existence of unique planetary forcing mechanism acting on the solar dynamo.

3.3 Toward a nonlinear solar dynamo with planetary forcing

The solar dynamo cannot be regarded as an isolated system, and the traditional view that treats it as an autonomous internal mechanism is therefore overly simplistic. As previously discussed, the conservation of angular momentum in a gravitationally bound system implies that,

$$\frac{dL_{\odot}}{dt} = \sum_{i} \frac{dL_{\odot,i}}{dt} \tag{6}$$

This relationship indicates that any change in planetary orbital angular momentum must be compensated by a corresponding variation in the Sun's rotational angular momentum, ensuring conservation of the total angular momentum of the system, as has been demonstrated for Earth's rotation and LOD variations (*eg.* Lopes *et al.* 2022, Lopes *et al.* 2022).

Even tiny changes in the Sun's rotation rate can lead to non-negligible effects in the dynamo process, via Coriolis force, shear, etc., given the dynamo's sensitivity. Radial, differential, and latitudinal components of solar rotation are modulated by the relative positions of the planets, which can be tracked through their $RA_{tot}(t)$. Importantly, $RA_{tot}(t)$ essentially encodes the direction of the net gravitational pull of the planets in the Sun's equatorial plane.

Within the Lagrangian and Virial formalism,

$$M_{tot} = L_{orb} + L_{spin},\tag{7}$$

with,

$$\frac{dM_{tot}}{dt} = 0. ag{8}$$

To investigate whether planetary dynamics can act as an external driver of the solar cycle, we employ a reduced dynamical system derived from the classical α - Ω dynamo theory (cf. equations 9). We adopt a low-order α - Ω dynamo model that corresponds to the leading temporal mode of the mean-field dynamo equations described by (Charbonneau & Sokoloff, 2023). In the full mean-field formulation, the poloidal A(t) and toroidal B(t) fields are governed by partial differential equations including spatial diffusion through Laplacian operators, meridional transport, and non-local source terms such as α -effect and the Ω -shear. When these equations are projected onto their fundamental dipolar mode in latitude and radius, the spatial dependence can be separated out, resulting in a set of coupled ordinary differential equations for the temporal amplitudes of the poloidal and toroidal components. In this reduced formulation, the Laplacian operator $-\eta \nabla^2$ is represented by linear damping terms (η_A, η_B) , while flux-loss and magnetic quenching are modeled through cubic non-linearities $(\mu_A A^3(t), \mu_B B^3(t))$. Likewise, the shearing term $\Omega(t) \frac{\partial A}{\partial \theta}$ reduces to a proportional coupling $\Omega_0 A(t)$, and the α -effect term $\alpha(B)B(t)$ becomes $\alpha_0 B(t)$.

This approach is widely used in dynamo theory (eg. Parker 1955, Weiss 1993, Knobloch & Landsberg 1996, Tobias et al. 1995) as it retains the essential nonlinear feedback loop responsible for magnetic field generation while allowing analytical insight and computational efficiency. Crucially, this low-order dynamical system remains phase-coherent and can respond to external perturbations, making it well suited for testing hypotheses of planetary forcing. The external terms $F_A(t)$ and $F_B(t)$, derived from the planetary right ascension and orbital angular momentum, thus represent physically motivated perturbations of the differential rotation and the α -effect, in full consistency with the mean-field dynamo framework. This external forcing is physically justified because RA(t) encodes the variations in the relative planetary orientation and therefore the barycentric torque exerted on the Sun (where $F_B(t) \propto RA(t)$). The term $F_B(t)$ represents the external modulation of the internal solar rotation, which directly alters the Ω -effect, specifically the $\Omega(t)A(t)$. In practice, we implemented RA(t) as a

time-varying factor modulating the Ω -term in the dynamo following equations,

$$\frac{dB}{dt} = \Omega(t)A(t) - \eta_B B(t) - \mu_B B(t)^3 + F_B(t)$$

$$\frac{dA}{dt} = \alpha_0 B(t) - \eta_A A(t) - \mu_A A(t)^3 + F_A(t)$$
(9)

where $\Omega(t) = \Omega_0 + \delta\Omega_{RA(t)}$ naturally enters the dynamo equation either as a multiplicative or additive forcing term, reflecting its role in modulating the generation of the toroidal magnetic field.

The temporal evolution of the solar cycle exhibits a remarkable phase coherence with planetary orbital motion when the latter is represented through the summed right ascension ($RA_{tot}(t)$, cf. Figure 8). Although $RA_{tot}(t)$ is purely geometric, it provides a direct measure of the barycentric orientation of the Solar System, which in turn modulates the Sun's angular momentum through conservation of total orbital and rotational momentum. When band-limited to the Schwabe range (8-13 years), $RA_{tot}(t)$ reveals an oscillatory (cf. Figure 8, blue curve) component that closely matches the periodicity of the sunspot cycle (cf. Figure 8, red curve). A systematic time-warping analysis demonstrates that the phase difference (cf. Figure 8, black curve, bottom panel) between $RA_{tot}(t)$ and the SSN evolves slowly and monotonically over centuries, indicating that the two signals share a persistent causal or dynamical linkage, but one that is non-stationary in time. Multiplying $RA_{tot}(t)$ by -1 only reflects a choice of dynamical convention: in an α - Ω dynamo, the effective sign of external forcing may be absorbed into the α or Ω coupling constants and does not alter the underlying physical mechanism.

This observation motivates the use of a low-order nonlinear α - Ω dynamo model, which represents the fundamental dipolar mode of the full mean-field dynamo equations described by Charbonneau & Sokoloff (2023). In this reduced formulation, spatial operators such as the Laplacian are projected onto their dominant eigenmode and replaced by linear damping, while magnetic quenching and buoyant flux loss are modeled by cubic nonlinear saturation terms. The model retains the essential dynamical structure of the solar dynamo-namely, generation of toroidal field by rotational shear (Ω -effect), regeneration of poloidal field by the α -effect, and nonlinear feedback-while allowing external forcing to be introduced in a controlled and physically meaningful manner.

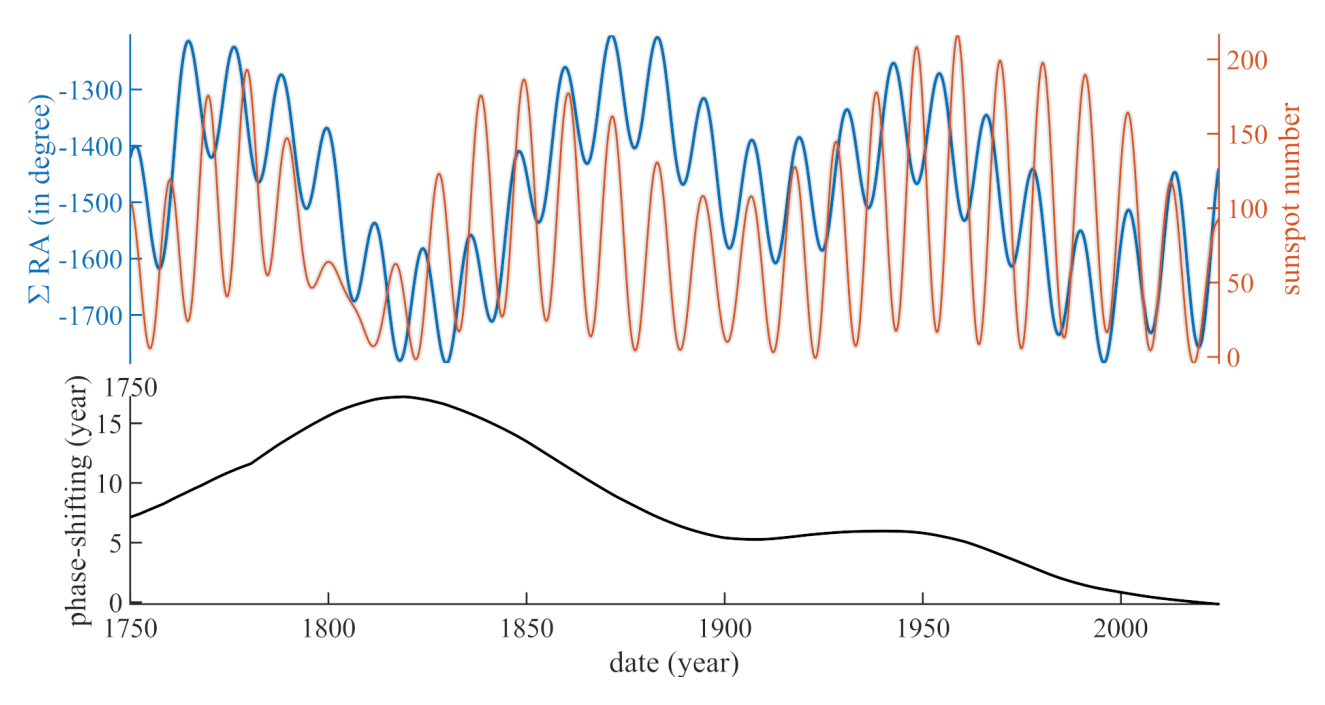


Figure 8: Top panel: superposition of the sunspot number time series (in red) and the smoothed, time-varying sum of planetary right ascensions (in blue), plotted with inverted polarity (multiplicative factor -1). Bottom panel: the instantaneous phase difference that evolves slowly over centuries. A clear visual correlation emerges between the two physical signals, particularly during the Dalton Minimum (∼1800–1830), thereby supporting the relevance of our simplified dynamo model.

The $RA_{tot}(t)$ signal acts as a driver on the toroidal and/or poloidal components, consistent with the theory of forced nonlinear oscillators. In this framework, the solar cycle emerges as a self-sustained oscillator operating near its natural frequency (11 years), while planetary forcing plays the role of a weak but coherent external modulator capable of locking the phase and shaping the long-term amplitude envelope. This approach thus provides the minimal dynamical system capable of translating observed planetary-solar phase coherence into a predictive physical mechanism (cf. Figure 9).

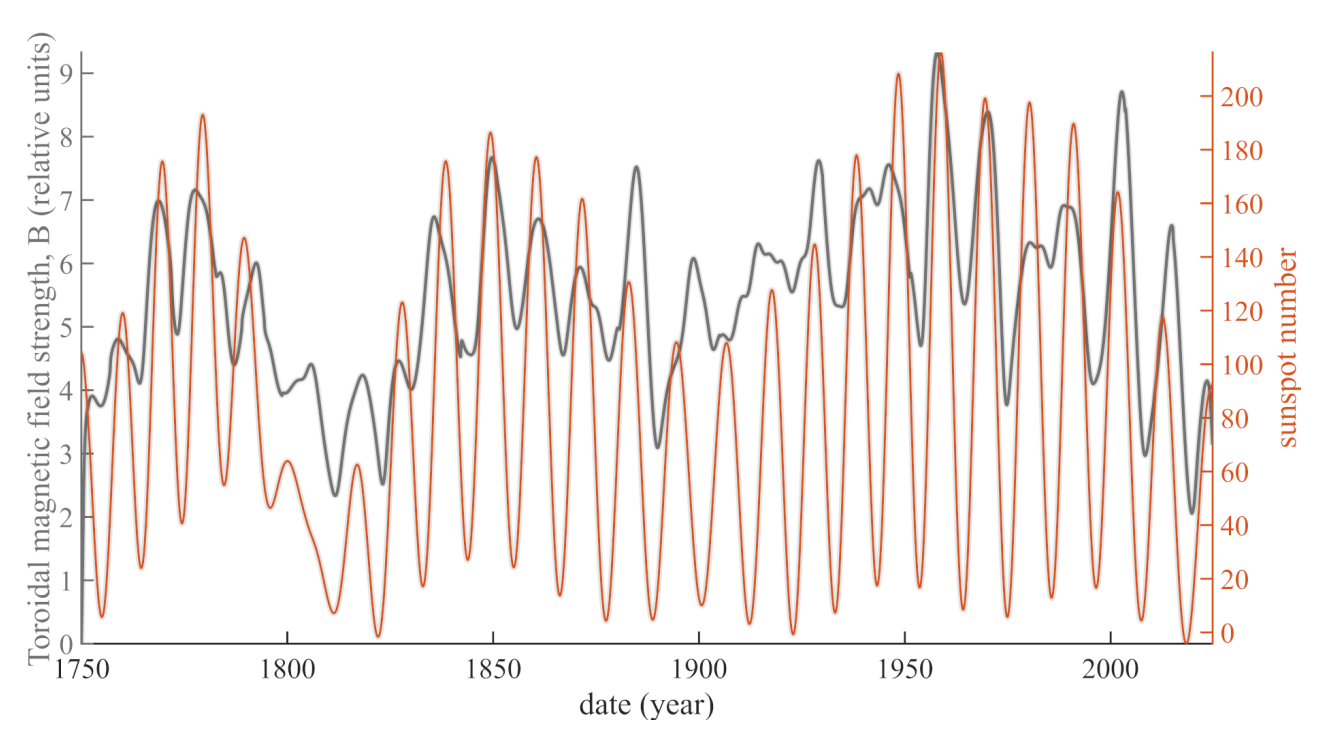


Figure 9: Superposition of the sunspot number time series (in red) and the toroidal magnetic field B(t) derived from our dynamo model (in gray; *cf.* Equations 9), driven solely by the summed planetary right ascensions. The envelope of the sunspot series is broadly reproduced, as are the Schwabe-cycle oscillations, despite the simplicity of the dynamo formulation and the use of a single external forcing mechanism.

Figure 9 compares the observed sunspot number (in red) with the toroidal magnetic field strength B(t) produced by our reduced dynamo model (in gray), which is forced solely by the sum of the planetary right ascensions. Despite the extreme simplicity of the model (cf. equations 9), consisting of only two coupled nonlinear ordinary differential equations, it reproduces the timing of individual solar cycles as well as the multi-decadal modulation of their amplitude. Notably, the major features of solar variability, such as the Dalton Minimum around 1800-1830 and the Modern Maximum in the mid-twentieth century, are clearly captured by the dynamo output. The relative decline in activity after Solar Cycle 19 is also reproduced, indicating that the model is sensitive to long-term changes encoded in the planetary forcing signal.

It is important to emphasize that the dynamo output B(t) is expressed in relative units and is not expected to match the sunspot number in absolute amplitude; instead, the relevant comparison lies in the coherence of phase and in the similarity of envelope modulation. The close correspondence visible in the figure demonstrates that the forcing derived from planetary orbital geometry contains sufficient information to drive the solar dynamo through phase locking. The consistency over nearly three centuries suggests that this agreement is not coincidental, but rather emerges from a deterministic relationship between planetary motion and the solar cycle. The absence of explicit internal stochastic forcing or data assimilation further strengthens this interpretation, as the solar-like behavior arises solely from the interaction between non-linear dynamo physics and an external, astronomically prescribed driver.

Overall, this figure provides compelling evidence that even a minimal α - Ω dynamo, when correctly forced and phasealigned, can reproduce the essential features of the observed sunspot record. This result directly supports the hypothesis that planetary forcing contributes to the modulation of the solar magnetic cycle.

4 Discussion

Our analyses reveal 11 pseudo-cycles common to both the sunspot number (SSN) and the length of day (LOD), jointly explaining about half of the total variance in each record (*cf.* Table 2; Figures 5 and 6). Their periods coincide with those derived from planetary orbital angular momenta and Laplace-type resonances (*cf.* Figures 3 and 4), and their cumulative distributions (*cf.* Figure 7) are statistically indistinguishable, ruling out random coincidence. Within a self-gravitating system, the Virial relation (*cf.* relation 1a) links kinetic and potential energies and constrains the exchange of angular momentum. Applied to the Sun-planet system, it implies that changes in planetary orbital configuration are balanced by opposite variations in the Sun's orbital or rotational motion. This establishes a deterministic coupling, whereby planetary dynamics modulate the Sun's rotation rate and, consequently, the solar dynamo.

Let us now examine the perturbative effect of the planets on system (cf. equations 9). As previously discussed at the beginning, the Sun is rotating with its own intrinsic angular momentum $\mathbf{L}_{\odot} = \mathbf{I}_{\odot} \Omega_{\odot}$ where \mathbf{I}_{\odot} is the effective moment of inertia of the Sun. Under the influence of a torque, ie. the sum of gravitational torques exerted by the planets (cf. Figure 2), then $\frac{d\mathbf{L}_{\odot}}{dt} = \boldsymbol{\tau}$. Assuming that \mathbf{I}_{\odot} remains approximately constant, ie. the solar radius does not vary significantly over the timescales considered, we obtain $\mathbf{I}_{\odot} \frac{d\Omega_{\odot}}{dt} = \boldsymbol{\tau}$. Using the values provided in Table 1, it is possible to roughly estimate the torque exerted by Jupiter alone (assuming a circular orbit and an offset barycenter). For the order of magnitude, let us take $\mathbf{r} \sim 4.48 \times 10^{11} m$, the lever arm, on the order of the solar radius \mathbf{R}_{\odot} (cf. Figure 3b) between the Sun and the barycenter is,

$$\|\mathbf{F}\| \approx \mathcal{G} \frac{M_{\odot} m_J}{r^2} \approx 6.67 \times 10^{-11} \times \frac{2 \times 10^{30} \times 1.9 \times 10^{27}}{(7.48 \times 10^{11})^2} \approx 4,76 \times 10^{23} N$$
 (10)

If the Sun is displaced from the barycenter by several tens of thousands of kilometers, typically up to $\sim 5 \times 10^7 m$, then,

$$\|\boldsymbol{\tau}\| \approx 4.76 \times 10^{23} \times 5 \times 10^7 \approx 2,38 \times 10^{31} N.m$$
 (11)

While this displacement is indeed large, it remains negligible in terms of angular variation when compared to the Sun's moment of inertia ($\mathbf{I}_{\odot} \approx \alpha M_{\odot} \mathbf{R}_{\odot}^2 \approx 5, 8 \times 10^{46} kg.m^2$).

Let.

$$\frac{d\Omega_{\odot}}{dt} = \frac{\tau}{\mathbf{I}_{\odot}},\tag{12}$$

then,

$$\|\frac{d\Omega_{\odot}}{dt}\| \approx \frac{2.38 \times 10^{31}}{5.8 \times 10^{46}} \approx 4.11 \times 10^{-16} rad. s^{-2}$$
(13)

Over a one-year, the resulting angular variation is,

$$\Delta\Omega_{\odot}|_{1year} = \|\frac{d\Omega_{\odot}}{dt}\| \times 3.157 \times 10^{7} \approx 1.29 \times 10^{-8} rad.s^{-1}$$
(14)

At the equator, the solar angular velocity is $\Omega_{\odot} \approx 2.9 \times 10^{-6} rad.s^{-1}$ (ie. 25-day period), then the ratio $\frac{\Delta\Omega_{\odot}|_{1\ year}}{\Omega_{\odot}}$ becomes,

$$\frac{\Delta\Omega_{\odot}|_{1 \ year}}{\Omega_{\odot}} \approx \frac{1.29 \times 10^{-8}}{2.9 \times 10^{-6}} \approx 0.45\% \tag{15}$$

This effect could naively be considered as cumulative over multiple cycles. If the Jupiter-Sun torque (and that of other planets) were to remain constant in both direction and amplitude over a period of 100 years, the resulting linear variation could exceed 45%, which would be enormous. However, this remark must be qualified. Over timescales of 10, 50, or 100 years, Jupiter completes several orbits around the Sun. The direction of the torque $\tau(t)$ changes continuously, so that the vectorial integration over a century does not lead to the linear accumulation described above. On the contrary, what occurs is an oscillatory behavior, including beat phenomena involving other planets (*eg.* Saturn). As a result, the Sun undergoes a much more modest oscillation of its rotation axis, ie, precession and nutation, than what would result from a simple linear acceleration accumulated over 100 years.

The torque acts not only on the amplitude of Ω_{\odot} but also on its direction, thereby inducing precession. The precession can be modeled by,

$$\frac{\Delta\Omega_{\odot}}{dt} = \Gamma \times \Omega_{\odot} \tag{16}$$

where Γ is a vector related to the torque τ . This simplified relation illustrates that the axis can slowly describe a conical motion around a mean direction. Nutation refers to an additional oscillation superimposed on the precessional motion. Changes in Ω_{\odot} , in either magnitude or inclination, primarily affect the tachocline, where velocity gradients are maximal. In the α - Ω dynamo model, this region plays a key role in winding the poloidal magnetic field into a toroidal one. Even a small perturbation $\delta\Omega$ can alter the shear rates () $\Delta\Omega$), slightly shift the latitudinal distribution of the magnetic field, or introduce a phase lag in the magnetic regeneration cycle. The amplification of the magnetic field in the tachocline region depends exponentially (in certain simplified models) on both the storage duration and the intensity of the shear. Even a few percent variation in Ω can significantly affect the final strength of the magnetic field.

If one considers only linear integration, the planetary torques induce very small variations in the magnitude of the solar rotation rate $|\Omega_{\odot}|$. However, when the system is evaluated in a fully vectorial framework, where both the sign and direction alternate over successive planetary configurations, especially due to the Jupiter-Saturn synodic cycle, any secular growth is

canceled. Instead, the system naturally gives rise to an oscillatory regime with beat frequencies, consistent with a slow precession/nutation of the solar rotation axis and a modulation of rotational shear within the tachocline. In a nonlinear α - Ω feedback dynamo, even small modulations (on the order of a few percent) in the differential rotation are sufficient to strongly affect the amplitude envelope of the toroidal magnetic field, due to the exponential sensitivity of dynamo efficiency to storage time and shear intensity. This prediction is directly supported by our reconstructions.

RA(t) represents the barycentric orientation (cf. Figure 8) of the Sun projected onto the solar equatorial plane; when appropriately weighted, it encodes the directional information of planetary torques that directly modulate the shear terms (Ω -effect) and/or the α -effect in the dynamo process. In contrast, L_{\odot} provides the global orbital amplitude, which is quasi-conserved, resulting in a smoother spectral signature compared to $RA_{tot}(t)$, while still exhibiting concordant periodicities. For this reason, we use $RA_{tot}(t)$ as a phase- and orientation-tracking signal, and L_{\odot} as an energetic baseline consistent with the conservation of total angular momentum.

The reduced-rank α - Ω dynamo model, when externally forced by $RA_{tot}(t)$, successfully reproduces both the Schwabe periodicity and the multi-decadal envelope, including the Dalton Minimum, the Modern Maximum, and the post-Solar Cycle 19 decline (cf. Figure 9). This behavior is characteristic of a phase-locked, self-sustained oscillator operating near its natural frequency and entrained by a weak yet coherent external forcing. The agreement over nearly three centuries, achieved without stochastic assimilation, supports a deterministic relationship between orbital geometry and the solar magnetic cycle.

A first recurrent objection asserts that planetary tidal forces are too weak to influence the Sun's internal dynamics. However, this critique relies on a linear and purely local assumption that is not applicable here. Our framework does not invoke static or localized tidal deformation, but rather a global modulation of solar rotation under the strict constraint of angular momentum conservation in the barycentric system. The induced torques, although small in instantaneous amplitude, act in a vectorial and oscillatory manner, modulating differential rotation within the tachocline, a region of extreme sensitivity in all α - Ω dynamo models.

A second objection suggests that correlations between solar activity and planetary characteristics may be coincidental. Yet, the convergence of three independent and mutually reinforcing signatures, namely: (i) almost exact co-periodicities extracted *via* Singular Spectrum Analysis (SSA); (ii) nearly identical cumulative distributions validated by the results of pairwise applications of the non-parametric two-sample Kolmogorov-Smirnov test; and (iii) correlations exceeding 0.999 for the eleven common periods, renders the hypothesis of chance statistically negligible.

A third criticism claims that $RA_{tot}(t)$ is merely a geometric construct without dynamical significance. In reality, $RA_{tot}(t)$ specifically represents the projection of the Sun's barycentric motion onto the solar equatorial plane, encoding the effective direction of the torque that modulates the orientation of the Sun's angular momentum and directly enters dynamo equations through the shear terms.

Finally, it is sometimes argued that variations in the terrestrial length-of-day have no physical connection with solar activity. However, the identification of eleven quasi-stationary components common to both LOD and SSN demonstrates

the presence of an external synchronizing agent acting simultaneously on Earth's rotation and the solar dynamo. Taken together, these points show that traditional objections, while historically reasonable within a Sun-as-isolated-body paradigm, are no longer applicable within a global Hamiltonian framework, where the Sun is treated as a dynamical component of the solar system in continuous exchange of angular momentum with the other orbiting bodies.

Our order-of-magnitude estimates assume circular planetary orbits and a stationary effective moment of inertia; they neglect fine-scale couplings such as internal radial variations and simplify the latitudinal distribution of differential rotation. From a methodological perspective, although the SSA algorithm has been carefully optimized, it may introduce small phase shifts when pseudo-periodic components exhibit significant overlap. Furthermore, the weighting of L_{\odot} inherently emphasizes the contribution of the Jovian giants, which may reduce the visibility of terrestrial components.

A central requirement of any robust theoretical framework lies in its ability to produce falsifiable predictions. The planetary forcing mechanism presented here satisfies this criterion by yielding multiple observable signatures that can be tested independently. First, phase locking between orbital dynamics, expressed through $RA_{tot}(t)$ and the barycentric angular momentum L_{\odot} and the solar cycle implies that the relative phase drift between the pseudo-periodic components extracted from the sunspot record must remain bounded and monotonic; a sudden loss of coherence or a phase reversal would constitute a critical test of the model. Second, modulations in tachocline shear are expected to manifest as torsional oscillations detectable by helioseismology, exhibiting periods corresponding to Laplace-type resonances and the combined Jupiter-Saturn synodic cycles. Third, the model predicts a directional modulation of the solar magnetic field, producing north-south asymmetries correlated with the orbital geometry encoded by $RA_{tot}(t)$, offering a direct observational test via hemispheric magnetic activity. Fourth, the multi-decadal envelope of solar variability, including the Dalton and Gleissberg minima, and the post-Solar Cycle 19 decline, should be reproducible a priori for future cycles using $RA_{tot}(t)$ and L_{\odot} as phase inputs alone, without resorting to empirical tuning or stochastic assimilation. Finally, from a methodological standpoint, the identification via SSA of stable components common to SSN, LOD, and L_☉ constitutes a built-in robustness criterion: the disappearance or fragmentation of these components under reasonable variations in SSA parameters (window length, embedding dimension, grouping criteria) would invalidate the hypothesis of a structurally imposed external forcing. Thus, rather than being speculative, our framework provides a coherent set of quantitative predictions that can be directly confronted with observations over forthcoming solar cycles.

Our results therefore suggest that the solar dynamo is not strictly autonomous, but instead operates as a weakly forced oscillator in which planetary configurations impose an external clock capable of phase-locking the cycle and modulating magnetic energy on long timescales. This framework naturally unifies the periodic signatures observed in the sunspot number (SSN), the terrestrial length of day (LOD), and barycentric quantities, while remaining fully consistent with the standard α - Ω dynamo physics.

We emphasize that the planetary forcing presented here is weak, it does not drive the solar cycle but rather tunes its phase and envelope. The solar dynamo undoubtedly involves internal chaotic processes as well; however, our results imply that it is not a purely self-determined system. Instead, it behaves like a weakly synchronized oscillator.

5 Conclusion

The present study demonstrates that the solar cycle bears clear imprints of planetary influence. Eleven common periodicities emerge in historical sunspot and LOD records, coinciding with those of planetary orbital resonances and the Sun's barycentric motion. Their coherence, confirmed by multiple independent analyses, points to a deterministic external clock regulating long-term solar variability.

By combining a Lagrangian-Virial formalism with a reduced α - Ω dynamo model, we show that a single planetary parameter, the summed right ascension RA(t), is sufficient to phase-lock the ~11-year Schwabe cycle and reproduce its multi-decadal modulation. The Sun thus behaves as a weakly synchronized oscillator, not as a fully autonomous system. Planetary configurations impose an external clock that modulates the phase and amplitude of magnetic activity while remaining fully compatible with standard dynamo physics.

This framework unifies solar activity, barycentric dynamics, and terrestrial rotation within a single dynamical system governed by angular-momentum conservation. It provides a set of quantitative, testable predictions, bounded phase drifts, resonance-specific torsional oscillations, hemispheric asymmetries, that future solar observations can directly evaluate. Confirming these signatures would firmly establish the role of celestial mechanics in solar variability; discrepancies would help delineate its limits.

Looking ahead, extending this Lagrangian-barycentric approach to 3-D dynamo simulations, other solar or stellar cycles, and coupled Sun-Earth interactions will clarify the generality of planetary synchronization. Whatever the outcome, the approach presented here offers a coherent, physically constrained pathway for integrating celestial mechanics into solar dynamo theory.

This work is dedicated to the memory of Jean-Louis Le Mouël, whose pioneering insights into geomagnetism, Earth rotation, and Sun-Earth coupling continue to inspire the exploration of deep connections between planetary dynamics and solar variability.

References

- Bartels, J. (1932). Terrestrial-magnetic activity and its relations to solar phenomena. *Terrestrial Magnetism and Atmospheric Electricity* 37(1), 1–52.
- Callebaut, D. K., C. de Jager, & S. Duhau (2012). The influence of planetary attractions on the solar tachocline. *Journal of atmospheric and solar-terrestrial physics* 80, 73–78.
- Chao, B. F., W. Chung, Z. Shih, & Y. Hsieh (2014). Earth's rotation variations: a wavelet analysis. *Terra Nova* 26(4), 260–264.
- Charbonneau, P. & D. Sokoloff (2023). Evolution of solar and stellar dynamo theory. Space Science Reviews 219(5), 35.
- Charvátová, I. (1988). The solar motion and the variability of solar activity. Advances in space research 8(7), 147-150.
- Cionco, R. G. & D. A. Pavlov (2018). Solar barycentric dynamics from a new solar-planetary ephemeris. *Astronomy & Astrophysics 615*, A153.
- Clausius, R. (1870). Ueber einen auf die wärme anwendbaren mechanischen satz. Annalen der Physik 217(9), 124–130.
- Courtillot, V. (1978). Sur une accélération récente de la variation séculaire du champ magnétique terrestre. *CR Hebd. SEances Acad. Sci. Paris* (287), 1095–1098.
- Courtillot, V., J.-B. Boulé, J.-L. L. Mouël, D. Gibert, P. Zuddas, A. Maineult, M. Gèze, & F. Lopes (2023). A living forest of tibetan juniper trees as a new kind of astronomical and geophysical observatory. *arXiv* preprint arXiv:2306.11450.
- Courtillot, V., J. Le Mouel, & P. Mayaud (1977). Maximum entropy spectral analysis of the geomagnetic activity index as over a 107-year interval. *Journal of Geophysical Research* 82(19), 2641–2649.
- Courtillot, V., J.-L. Le Mouël, F. Lopes, & D. Gibert (2022). On sea-level change in coastal areas. *Journal of Marine Science and Engineering 10*(12), 1871.
- Courtillot, V., F. Lopes, & J. Le Mouël (2021). On the prediction of solar cycles. Solar Physics 296, 1–23.
- Currie, R. G. (1966). The geomagnetic spectrum—40 days to 5.5 years. *Journal of Geophysical Research* 71(19), 4579–4598.
- del Rio, R. A., D. Gambis, D. Salstein, P. Nelson, & A. Dai (2003). Solar activity and earth rotation variability. *Journal of Geodynamics* 36(3), 423–443.
- Diodato, N. & G. Bellocchi (2024). Millennium-scale changes in the atlantic multidecadal oscillation influenced groundwater recharge rates in italy. *Communications Earth & Environment* 5(1), 56.
- Duan, P., G. Liu, L. Liu, X. Hu, X. Hao, Y. Huang, Z. Zhang, & B. Wang (2015). Recovery of the 6-year signal in length of day and its long-term decreasing trend. *Earth, Planets and Space* 67, 1–11.
- Dumont, S., J. d. B. d'Ars, J.-B. Boulé, V. Courtillot, M. Gèze, D. Gibert, V. Kossobokov, J.-L. L. Mouël, F. Lopes,
 M. C. Neves, et al. (2025). On a planetary forcing of global seismicity. Frontiers in Earth Sciences, Section Solid Earth Geophysics 13.

- Eddy, J. A., R. L. Gilliland, & D. V. Hoyt (1982). Changes in the solar constant and climatic effects. *Nature 300*(5894), 689–693.
- Fairbridge, R. W. & J. H. Shirley (1987). Prolonged minima and the 179-yr cycle of the solar inertial motion. *Solar Physics 110*, 191–210.
- Gardner, W. A. (1993). Cyclic wiener filtering: theory and method. *IEEE Transactions on communications* 41(1), 151–163.
- Gleissberg, W. (1939). A long-periodic fluctuation of the sun-spot numbers. *The Observatory, Vol. 62, p. 158-159* (1939) 62, 158–159.
- Hale, G. E., F. Ellerman, S. B. Nicholson, & A. H. Joy (1919). The magnetic polarity of sun-spots. *Astrophysical Journal*, vol. 49, p. 153 49, 153.
- Holme, R. & O. De Viron (2013). Characterization and implications of intradecadal variations in length of day. *Nature* 499(7457), 202–204.
- Horstmann, G. M., G. Mamatsashvili, A. Giesecke, T. V. Zaqarashvili, & F. Stefani (2023). Tidally forced planetary waves in the tachocline of solar-like stars. *The Astrophysical Journal 944*(1), 48.
- Hung, C.-C. (2007). Apparent relations between solar activity and solar tides caused by the planets. Technical report.
- Jose, P. D. (1965). Sun's motion and sunspots. Astronomical Journal, Vol. 70, p. 193 70, 193.
- Kasatkina, E., O. Shumilov, & M. Krapiec (2007). On periodicities in long term climatic variations near 68 n, 30 e. *Advances in Geosciences 13*, 25–29.
- Knobloch, E. & A. Landsberg (1996). A new model of the solar cycle. *Monthly Notices of the Royal Astronomical Society* 278(1), 294–302.
- Kuhn, J., K. Libbrecht, & R. Dicke (1988). The surface temperature of the sun and changes in the solar constant. *Science* 242(4880), 908–911.
- Lagrange, J. L. (1788). Mécanique analytique. Mallet-Bachelier.
- Lambeck, K. (2005). The Earth's variable rotation: geophysical causes and consequences. Cambridge University Press.
- Landau, L. D. & E. M. Lifshitz (2000). *Mechanics, The Classical Course of Theoretical Physics, volume 1, 3th ed.*Butterworth-Heinemann edition: Oxford, UK.
- Laplace, P.-S. (1799). Traité de mécanique céleste, Volume 1 et 2. De l'imprimerie de Crapelet.
- Latt, W., U.-X. Tan, K. Veluvolu, C. Shee, & W. Ang (2009). Real-time estimation and prediction of periodic signals from attenuated and phase-shifted sensed signals. Dans 2009 IEEE/ASME International Conference on Advanced Intelligent Mechatronics, pp. 1643–1648. IEEE.
- Le Mouël, J., D. Gibert, V. Courtillot, S. Dumont, J. de Bremond d'Ars, S. Petrosino, P. Zuddas, F. Lopes, J.-B. Boulé, M. Neves, *et al.* (2023). On the external forcing of global eruptive activity in the past 300 years. *Frontiers in Earth Science 11*, 1254855.

- Le Mouël, J., F. Lopes, & V. Courtillot (2020a). Solar turbulence from sunspot records. *Monthly Notices of the Royal Astronomical Society* 492(1), 1416–1420.
- Le Mouël, J., F. Lopes, V. Courtillot, & D. Gibert (2019). On forcings of length of day changes: From 9-day to 18.6-year oscillations. *Physics of the Earth and Planetary Interiors* 292, 1–11.
- Le Mouël, J.-L., V. Kossobokov, & V. Courtillot (2010). A solar pattern in the longest temperature series from three stations in europe. *Journal of Atmospheric and Solar-Terrestrial Physics* 72(1), 62–76.
- Le Mouël, J.-L., F. Lopes, & V. Courtillot (2017). Identification of gleissberg cycles and a rising trend in a 315-year-long series of sunspot numbers. *Solar Physics* 292(3), 43.
- Le Mouël, J.-L., F. Lopes, & V. Courtillot (2019). A solar signature in many climate indices. *Journal of Geophysical Research: Atmospheres* 124(5), 2600–2619.
- Le Mouël, J.-L., F. Lopes, & V. Courtillot (2020b). Characteristic time scales of decadal to centennial changes in global surface temperatures over the past 150 years. *Earth and Space Science* 7(4), e2019EA000671.
- Le Mouël, J.-L., F. Lopes, V. Courtillot, D. Gibert, & J.-B. Boulé (2023). Is the earth's magnetic field a constant? a legacy of poisson. *Geosciences* 13(7), 202.
- Li, K., W. Feng, J. Xu, P. Gao, L. Yang, H. Liang, & L. Zhan (2012). Why is the solar constant not a constant? *The Astrophysical Journal* 747(2), 135.
- Lopes, F., V. Courtillot, D. Gibert, & J.-L. L. Mouël (2022). On two formulations of polar motion and identification of its sources. *Geosciences* 12(11), 398.
- Lopes, F., V. Courtillot, D. Gibert, J.-L. L. Mouël, & J.-B. Boulé (2022). On distributions law of planetary rotations and revolutions as a function of aphelia, following lagrange's formulation. *arXiv preprint arXiv:2209.07213*.
- Lopes, F., D. Gibert, V. Courtillot, J.-L. L. Mouël, & J.-B. Boulé (2024). On the optimization of singular spectrum analyses: A pragmatic approach. *arXiv preprint arXiv:2412.17793*.
- Lopes, F., J. Le Mouël, V. Courtillot, & D. Gibert (2021). On the shoulders of laplace. *Physics of the Earth and Planetary Interiors 316*, 106693.
- Lopes, F., J.-L. Le Mouël, & D. Gibert (2017). The mantle rotation pole position. a solar component. *Comptes Rendus*. *Géoscience 349*(4), 159–164.
- Mörth, H. & L. Schlamminger (1979). Planetary motion, sunspots and climate. Dans *Solar-Terrestrial Influences on Weather and Climate: Proceedings of a Symposium/Workshop held at the Fawcett Center for Tomorrow, The Ohio State University, Columbus, Ohio, 24–28 August, 1978*, pp. 193–207. Springer.
- Mufti, S. & G. Shah (2011). Solar-geomagnetic activity influence on earth's climate. *Journal of Atmospheric and Solar-Terrestrial Physics* 73(13), 1607–1615.
- Mursula, K., I. Usoskin, & B. Zieger (1997). On the claimed 5.5-year periodicity in solar activity. *Solar Physics* 176, 201–210.
- Parker, E. N. (1955). Hydromagnetic dynamo models. Astrophysical Journal, vol. 122, p. 293 122, 293.

- Perryman, M. & T. Schulze-Hartung (2011). The barycentric motion of exoplanet host stars-tests of solar spin-orbit coupling. *Astronomy & Astrophysics* 525, A65.
- Pouillet, C. S. (1837). 'déterminations des basses températures au moyen du pyrometre aair, du pyrometre magnétique et du thermometre aalcool. *Comptes rendus hebdomadaines 4*, 513–519.
- Ptitsyna, N. & I. Demina (2021). Solar-activity cycles reconstructed from statistics on polar lights with allowance for the contribution of the main magnetic field of the earth in 1000–2000. *Geomagnetism and Aeronomy 61*, 312–324.
- Ray, R. D. & S. Y. Erofeeva (2014). Long-period tidal variations in the length of day. *Journal of Geophysical Research: Solid Earth 119*(2), 1498–1509.
- Richards, M. T., M. L. Rogers, & D. S. P. Richards (2009). Long-term variability in the length of the solar cycle. *Publications of the Astronomical Society of the Pacific 121*(881), 797.
- Rosen, R. D. & D. A. Salstein (1983). Variations in atmospheric angular momentum on global and regional scales and the length of day. *Journal of Geophysical Research: Oceans* 88(C9), 5451–5470.
- Scafetta, N. (2012). Multi-scale harmonic model for solar and climate cyclical variation throughout the holocene based on jupiter–saturn tidal frequencies plus the 11-year solar dynamo cycle. *Journal of Atmospheric and Solar-Terrestrial Physics* 80, 296–311.
- Scafetta, N. (2014). The complex planetary synchronization structure of the solar system. *arXiv preprint* arXiv:1405.0193.
- Scafetta, N. & A. Bianchini (2022). The planetary theory of solar activity variability: a review. *Frontiers in Astronomy and Space Sciences* 9, 937930.
- Scafetta, N., F. Milani, & A. Bianchini (2020). A 60-year cycle in the meteorite fall frequency suggests a possible interplanetary dust forcing of the earth's climate driven by planetary oscillations. *Geophysical Research Letters* 47(18), e2020GL089954.
- Schove, D. J. (1947). The sunspot-cycle before 1750. Terrestrial Magnetism and Atmospheric Electricity 52(2), 233–238.
- Schwabe, H. (1844). Sonnenbeobachtungen im jahre 1843. von herrn hofrath schwabe in dessau. *Astronomische Nachrichten, volume 21, issue 15, p. 233 21*, 233.
- Seker, I. (2013). Are planetary tides on the sun and the birthplace of sunspots related? Solar Physics 286, 303–314.
- Seymour, P., M. Willmott, & A. Turner (1992). Sunspots, planetary alignments and solar magnetism: a progress review. *Vistas in astronomy 35*, 39–71.
- Shirley, J. H. (2023). Orbit-spin coupling, the solar dynamo, and the planetary theory of sunspots. *arXiv preprint arXiv:2309.13076*.
- Sidorenkov, N. (2017). Synchronization of terrestrial processes with frequencies of the earth-moon-sun system. *Astronomical and Astrophysical Transactions* 30(2), 249–260.
- Smythe, C. M. & J. A. Eddy (1977). Planetary tides during the maunder sunspot minimum. *Nature* 266(5601), 434–435.

- Stefani, F., A. Giesecke, N. Weber, & T. Weier (2016). Synchronized helicity oscillations: A link between planetary tides and the solar cycle? *Solar Physics* 291(8), 2197–2212.
- Stefani, F., A. Giesecke, & T. Weier (2019). A model of a tidally synchronized solar dynamo. Solar Physics 294(5), 60.
- Stefani, F., G. Horstmann, M. Klevs, G. Mamatsashvili, & T. Weier (2024). Rieger, schwabe, suess-de vries: The sunny beats of resonance. *Solar Physics* 299(4), 51.
- Stefani, F., R. Stepanov, & T. Weier (2021). Shaken and stirred: when bond meets suess-de vries and gnevyshev-ohl. *Solar Physics* 296(6), 88.
- Tobias, S., N. Weiss, & V. Kirk (1995). Chaotically modulated stellar dynamos. *Monthly Notices of the Royal Astronomi-* cal Society 273(4), 1150–1166.
- Trofimov, D., S. Petrov, P. Movsesyan, K. Zheltova, & V. Kiyaev (2021). Recent acceleration of the earth rotation in the summer of 2020: Possible causes and effects. Dans *Journal of Physics: Conference Series*, Volume 2103, pp. 012039. IOP Publishing.
- Tsichla, M., M. Gerontidou, & H. Mavromichalaki (2019). Spectral analysis of solar and geomagnetic parameters in relation to cosmic-ray intensity for the time period 1965–2018. *Solar Physics* 294, 1–18.
- Usoskin, I. G. (2017). A history of solar activity over millennia. Living Reviews in Solar Physics 14(1), 3.
- Veretenenko, S. & M. Ogurtsov (2018). 60-year cycle in the earth's climate and dynamics of correlation links between solar activity and circulation of the lower atmosphere. *Geomagnetism and Aeronomy* 58, 973–981.
- Wagner, G., J. Beer, J. Masarik, R. Muscheler, P. W. Kubik, W. Mende, C. Laj, G. M. Raisbeck, & F. Yiou (2001). Presence of the solar de vries cycle (205 years) during the last ice age. *Geophysical Research Letters* 28(2), 303–306.
- Weiss, N. (1993). Solar and stellar dynamos. Dans *Physics of Solar and Stellar Coronae: GS Vaiana Memorial Symposium: Proceedings of a Conference of the International Astronomical Union, Held in Palermo, Italy, 22–26 June, 1992*, pp. 541–547. Springer.
- Willett, H. C. (1962). The relationship of total atmospheric ozone to the sunspot cycle. *Journal of Geophysical Research* 67(2), 661–670.
- Wolf, R. (1859). Extract of a letter to mr. carrington. *Monthly Notices of the Royal Astronomical Society, Vol. 19*, p. 85-86 19, 85-86.
- Wood, R. M. & K. D. Wood (1965). Solar motion and sunspot comparison. *Nature* 208(5006), 129–131.
- Xiao, M., T. Jin, H. Ding, L. Yang, X. Li, & J. Li (2025). The global 64-year sea level oscillation and its possible external excitation sources. *Science China Earth Sciences* 68(3), 898–908.
- Zaccagnino, D., F. Vespe, & C. Doglioni (2020). Tidal modulation of plate motions. Earth-science reviews 205, 103179.

Appendix A The Virial theorem

The Virial theorem (from the Latin vis, meaning 'force') was proposed by Clausius (1870). We present it in this appendix.

Statement. The Virial theorem relates the average kinetic energy $\langle T \rangle$ and the average potential energy $\langle U \rangle$ of a mechanical system. In the particular case where the force derives from a homogeneous potential of degree n, it can be stated as follows,

$$2\langle T \rangle = n\langle U \rangle \tag{A.01}$$

This means that, on average (in the sense of a long-term time average or an ensemble average), the kinetic and potential energies are not independent, but obey a proportional relationship, the factor of which depends on the degree of homogeneity of the potential. In the case of the Newtonian gravitational potential, which follows a $\frac{1}{r}$ law (*ie.* a potential of degree -1), we have,

$$2\langle T \rangle = -1\langle U \rangle \Rightarrow 2\langle T \rangle + \langle U \rangle = 0 \Rightarrow \langle T \rangle = -\frac{1}{2}\langle U \rangle \tag{A.02}$$

Proof. Consider a system of N particles with masses m_i , positions \mathbf{r}_i , and velocities \mathbf{v}_i , for i = 1, ..., N. The total kinetic energy is given by,

$$T = \sum_{i=1}^{N} \frac{1}{2} m_i ||\mathbf{v}_i||^2, \tag{A.03}$$

and the total potential energy (sum of the interaction potentials) is given by,

$$U = \sum_{i=1}^{N} U_i(\mathbf{r}_1, \mathbf{r}_2, \dots, \mathbf{r}_N), \tag{A.04}$$

where each U_i depends on the positions (in the Newtonian case, pairwise interaction energies are summed). We introduce the virial quantity G(t), defined by,

$$G(t) = \sum_{i=1}^{N} m_i \mathbf{r}_i \cdot \mathbf{v}_i = \sum_{i=1}^{N} m_i \mathbf{r}_i \cdot \dot{\mathbf{r}}_i$$
(A.05)

where \cdot denotes the dot product and $\dot{\mathbf{r}}_i = \mathbf{v}_i$. We now compute the time derivative $\frac{dG}{dt}$ of relation (A.05),

$$\frac{dG}{dt} = \sum_{i=1}^{N} m_i (\dot{\mathbf{r}}_i \cdot \dot{\mathbf{r}}_i + \mathbf{r}_i \cdot \ddot{\mathbf{r}}_i). \tag{A.06}$$

Noting that $\dot{\mathbf{r}}_i \cdot \dot{\mathbf{r}}_i = ||\mathbf{v}_i||^2$ and that $\dot{\mathbf{r}}_i \cdot \ddot{\mathbf{r}}_i = \dot{\mathbf{r}}_i \cdot \dot{\mathbf{a}}_i$, the previous expression becomes,

$$\frac{dG}{dt} = \sum_{i=1}^{N} m_i ||\mathbf{v}_i||^2 + \sum_{i=1}^{N} m_i \mathbf{r}_i \cdot \mathbf{a}_i$$
(A.07)

The first term corresponds to twice the kinetic energy, up to a factor of $\frac{1}{2}$,

$$\sum_{i=1}^{N} m_i ||\mathbf{v}_i||^2 = 2T. \tag{A.08}$$

It thus remains to examine the second term. Newton's second law tells us that $\mathbf{F}_i = m_i \mathbf{a}_i$,

$$\mathbf{r}_i \cdot \mathbf{a}_i = \frac{1}{m_i} \mathbf{r}_i \cdot \mathbf{F}_i, \tag{A.09}$$

thus, we can write,

$$\sum_{i=1}^{N} m_i \mathbf{r}_i \cdot \mathbf{a}_i = \sum_{i=1}^{N} \mathbf{r}_i \cdot \mathbf{F}_i. \tag{A.10}$$

If the force derives from a potential $U(r_1, \ldots, r_N)$, we have

$$\mathbf{F}_i = -\nabla_{\mathbf{r}_i} U,\tag{A.11}$$

and consequently,

$$\sum_{i=1}^{N} \mathbf{r}_{i} \cdot \mathbf{F}_{i} = -\sum_{i=1}^{N} \mathbf{r}_{i} \cdot \nabla_{\mathbf{r}_{i}} U. \tag{A.12}$$

If the potential is homogeneous of degree n, this means that,

$$U(\lambda \mathbf{r}_1, \dots \lambda \mathbf{r}_N) = \lambda^N(\mathbf{r}_1, \dots, \mathbf{r}_N) \quad \forall \lambda > 0$$
(A.13)

Applying Euler's theorem on homogeneous functions, we obtain,

$$\sum_{i=1}^{N} \mathbf{r}_{i} \cdot \nabla_{\mathbf{r}_{i}} U = nU \tag{A.14}$$

Indeed, the gradient $\nabla_{\mathbf{r}_i}U$ behaves as a homogeneous function of degree n-1, and so on. Combining this with the negative sign in the force expression, we obtain,

$$\sum_{i=1}^{N} \mathbf{r}_i \cdot \mathbf{F}_i = -nU. \tag{A.15}$$

Substituting all of this back into relation (A.06), the expression for $\frac{dG}{dt}$ becomes,

$$\frac{dG}{dt} = 2T + \sum_{i=1}^{N} \mathbf{r}_i \cdot \mathbf{F}_i = 2T - nU. \tag{A.16}$$

If the system is in equilibrium, or if it is periodic and we take the average over one or several periods, the average derivative $\langle \frac{dG}{dt} \rangle$ is zero. In other words, $\langle G(t) \rangle$ does not increase or decrease over the long term. This leads to the condition,

$$0 = 2\langle T \rangle - n \langle U \rangle \Rightarrow 2\langle T \rangle = n \langle U \rangle \tag{A.17}$$

For a self-gravitating system (eg. a star cluster, a simplified planetary system, etc.), the Newtonian potential is proportional to $\frac{1}{r}$, which corresponds to a homogeneity degree of n = -1. Indeed $\forall \lambda > 1$,

$$U(\lambda \mathbf{r}) \propto \sum_{i \neq j} = \frac{1}{\|\lambda \mathbf{r}_i - \lambda \mathbf{r}_j\|} = \frac{1}{\lambda} \sum_{i \neq j} \frac{1}{\|\mathbf{r}_i - \mathbf{r}_j\|}.$$
(A.18)

The Virial Theorem then yields,

$$2\langle T \rangle = -1\langle U \rangle \Rightarrow 2\langle T \rangle + \langle U \rangle = 0 \tag{A.19}$$

On long-term average, we obtain $\langle T \rangle = -\frac{1}{2} \langle U \rangle$ and thus, denoting the total energy by $\langle E \rangle = \langle T \rangle + \langle U \rangle$, we classically arrive at $\langle E \rangle = -\langle T \rangle$.

Appendix B The total exchange of angular momentum sums to zero

Let us begin by taking the time derivative of equation (1b),

$$\frac{dM_{tot}}{dt} = \sum_{i=1}^{N} \left[\frac{d}{dt} m_i(\mathbf{r}_i \times \mathbf{v}_i) \right) + \frac{d}{dt} (I_i \mathbf{\Omega}_i))$$
(B.01)

For each body, the orbital angular momentum is given by $M_{orb,i} = m_i(\mathbf{r}_i \times \mathbf{v}_i)$ whose time derivative is written as,

$$\frac{d}{dt}(m_i(\mathbf{r}_i \times \mathbf{v}_i)) = m_i(\frac{d}{dt}(\mathbf{r}_i) \times \mathbf{v}_i + \mathbf{r}_i \times \frac{d}{dt}(\mathbf{v}_i))$$
(B.02)

In $\frac{d}{dt}(\mathbf{r}_i)$, we recognize \mathbf{v}_i so the first term becomes $\mathbf{v}_i \times \mathbf{v}_i = 0$. The second term, $\mathbf{r}_i \times \frac{d}{dt}(\mathbf{v}_i)$, involves the total force applied to the ith planet,

$$m_i = \frac{d\mathbf{v}_i}{dt} = \mathbf{F}_i \Rightarrow \mathbf{r}_i \times \frac{d\mathbf{v}_i}{dt} = \frac{1}{m_i} (\mathbf{r}_i \times \mathbf{F}_i)$$
 (B.03)

Equation (B.02) simply becomes,

$$\frac{d}{dt}(m_i(\mathbf{r}_i \times \mathbf{v}_i)) = \mathbf{r}_i \times \mathbf{F}_i. \tag{B.04}$$

If there is no external force, *ie.* from outside the Solar System, \mathbf{F}_i is essentially the sum of internal gravitational forces, plus small torques due to the rotation of other bodies, *etc*. One could rewrite \mathbf{F}_i as $\sum_{j\neq i} \mathbf{F}_{ij}$.

For the rotational component of each planet, we have,

$$M_{rot,i} = I_i \Omega_i$$
 (B.05)

In most rigid-body problems, I_i is considered constant, ie no significant internal deformation. Then,

$$\frac{d}{dt}(I_i\Omega_i) = I_i \frac{d\Omega_i}{dt} = \Gamma_i,$$
(B.06)

where Γ_i corresponds to the torque exerted on the ith planet. For example, may result from the gravitational attraction of another planet acting on an inertia bulge, *etc*. We thus obtain for the time derivative of equation (B.05)

$$\frac{dM_{rot,i}}{dt} = I_i \frac{d\Omega_i}{dt} = \Gamma_i, \tag{B.07}$$

under the assumption $I_i \approx const$. By adding the orbital (B.04) and rotational (B.07) components, the time derivative of the angular momentum for the i^{th} planet becomes,

$$\frac{d}{dt}[m_i(\mathbf{r}_i \times \mathbf{v}_i) + I_i\Omega_i] = \mathbf{r}_i \times \mathbf{F}_i + \Gamma_i.$$
(B.08)

Therefore, we have,

$$\frac{dM_{tot}}{dt} = \sum_{i=1}^{N} (\mathbf{r}_i \times \mathbf{F}_i + \Gamma_i). \tag{B.09}$$

If the system is closed, the sum of internal forces \mathbf{F}_i , taken in pairs satisfies,

$$\sum_{i=1}^{N} \mathbf{r}_i \times \mathbf{F}_i = 0, \tag{B.10}$$

and the sum of internal torques Γ_i is also zero when all mutual gravitational and torque interactions are taken into account,

$$\sum_{i=1}^{N} \Gamma_i = 0. \tag{B.11}$$

In practice, the torque Γ_i acting on the ith planet body is the reaction to a torque $-\Gamma_i$ exerted on another jth body. Thus,

$$\frac{dM_{tot}}{dt} = 0. ag{B.12}$$

Hence, if one of the terms $M_{orb,i}$ varies, there must necessarily be a compensation in one or more terms $M_{rot,j}$ or $M_{orb,j}$, so that the total sum remains unchanged. In other words, as soon as a torque Γ_i modifies the rotation of i^{th} planet, it corresponds to a force (or torque) equal and opposite acting on another element of the system (another planet, or the Sun), thereby modifying its orbital angular momentum or its spin, and so on. This is often expressed as the total exchange of angular momentum sums to zero. Concretely, one can write,

$$\Gamma_i = \frac{dM_{rot,i}}{dt} = -\frac{dM_{rot,j}}{dt} \Longleftrightarrow \sum_i \frac{dM_{tot,i}}{dt} = 0$$
(B.13)

Appendix C The too-good-to-fit arguments

Here we investigate the similarity between the ranked distributions of periodicities extracted from SSN, LOD, and L_{\odot} plus LR* series associated with the planetary Laplace-type resonances listed in the last column of Table 2.

First of all, the correlations in between the SSN, LOD, L_{\odot} , and LR* series listed in Table C1 are unexpectedly high. We compared the observed correlations to those obtained in 3400 bootstrap simulations, which account for exponentially distributed periods. Each set of eleven random periods was ordered and then participated in evaluation of correlation coefficient, r. The observed correlations in between the SSN, LOD, are L_{\odot} are higher than the maximum in simulations of 3400 surrogate pairs, $r_{max} = 0.9966$, while the observed correlations of the 11 reference periods LR* with others were exceeded in 1, 5, and 15 cases out of 3400 simulations. This allows us to conclude that the coincidences are not random with confidence above 99%, at least.

	SSN	LOD	${ m L}_{\odot}$	LR*
SSN	11	0.000294	0.000294	0.000588
LOD	0.999154	11	0.000294	0.001765
${\rm L}_{\odot}$	0.012941	0.998874	11	0.004706
LR*	0.995975	0.995629	0.99343	11

Table C1: Pairwise correlation statistics: the observed correlation coefficients, r (under the diagonal), number of periods (on the diagonal), and the empirical probability of obtaining an equal or larger r by chance under a null hypothesis of ordered exponentially distributed random series (above the diagonal).

Secondly, we applied pairwise the two-sample Kolmogorov-Smirnov test to the periods extracted from SSN, LOD, L_{\odot} data, and LR* series. As is evident from Figure 7, the maximum absolute difference between their empirical cumulative distribution functions, $D_{11,11}$, is less than 0.1, so that $\lambda_{K-S} < 0.1 * (11/2)^{0.5} = 0.2345$, which value corresponds to the probability $\alpha < 3 \times 10^{-6}$ to reject the null hypothesis that both samples originate from the same continuous distribution, implying, with confidence $(1 - \alpha) = 99.9997\%$, that the ranked periodicities across the physical quantities considered follow almost identical cumulative distribution.

Thus, such a too-good-to-fit behavior of the SSN, LOD, L_{\odot} , and LR* periodicities is unlikely to arise by chance from independent processes and instead suggests a strong underlying constraint linking these datasets. We interpret this as further evidence that the pseudo-periodicities identified by SSA share a common physical origin, most plausibly related to planetary Laplace-type resonances within the Solar System's dynamical framework.